Non-NMDA glutamate receptor occupancy and open probability at a rat cerebellar synapse with single and multiple release sites

R. Angus Silver, Stuart G. Cull-Candy and Tomoyuki Takahashi*

*Department of Pharmacology, University College London, Gower Street, London WC1E 6BT, UK and *Department of Neurophysiology, Institute for Brain Research, Faculty of Medicine, University of Tokyo, Hongo 113, Tokyo, Japan*

1. Excitatory postsynaptic currents (EPSCs) were recorded under whole-cell voltage clamp from granule cells in slices of rat cerebellum. EPSCs from individual mossy fibre inputs were identified by their all-or-none appearance in response to a graded stimulus. Excitatory synaptic transmission was investigated at room temperature (~24 °C) and at near-physiological temperature (~34 °C) by analysing current fluctuations in the peak and decay of the non-*N*-methyl-D-aspartate (non-NMDA) component of EPSCs.

2. In a subset of synapses the mean EPSC amplitude remained unchanged as the probability of transmitter release was substantially lowered by raising the extracellular [Mg^{2+}] and lowering [Ca^{2+}]. These synapses were considered to have only one functional release site. Single-site synapses had small EPSCs (139 ± 16 pS, $n = 5$, at 24 °C) with a large coefficient of variation (c.v. = 0·23 ± 0·02, $n = 5$) and an amplitude distribution that was well fitted by a Gaussian distribution in four out of five cases. The EPSC latency had a unimodal distribution and its standard deviation had a temperature dependence with a temperature coefficient (Q_{10}; range, 24–35 °C) of 2·4 ± 0·4 ($n = 4$).

3. Peak-scaled non-stationary fluctuation analysis of single-site EPSCs indicated that the mean conductance of the underlying non-NMDA channels was 12 ± 2 pS ($n = 4$) at 35 °C. Upper and lower limits for mean channel open probability (P_o), calculated from fluctuations in the EPSC peak amplitude, were 0·51 and 0·38, respectively. These estimates, together with the open probability of the channel when bound by transmitter, suggest that only about 50% of the non-NMDA channels were occupied following the release of a quantum of transmitter.

4. At some multi-site synapses EPSCs had a low c.v. (0·04 ± 0·01, $n = 5$) at 34 °C and non-stationary fluctuation analysis gave a parabolic variance–mean current relationship. This suggests that practically all of the non-NMDA receptors were occupied by glutamate at the peak of the EPSC. The channel open probability ($P_o = 0·84 \pm 0·03$, $n = 5$) at these 'saturated' multi-site synapses will therefore equal the open probability of the channel when bound by transmitter ($P_{o,max}$).

5. Non-stationary fluctuation analysis of EPSCs from 'saturating' multi-site synapses indicated that 170 ± 40 postsynaptic non-NMDA channels were exposed to transmitter at the peak of the EPSC. The mean conductance of the synaptic channels was 10 ± 2 pS ($n = 5$) at 34 °C.

6. At synapses with multiple release sites the EPSC decay time became faster when release probability was lowered (by reducing the external [Ca^{2+}]/[Mg^{2+}] ratio), indicating that the transmitter concentration profile depended on release probability. No such speeding of the EPSC decay was observed at single-site synapses.

7. Our results suggest that release of a packet of transmitter from a single release site does not saturate postsynaptic non-NMDA receptors at cerebellar mossy fibre–granule cell synapses. However, at multi-site synapses transmitter released from neighbouring sites can overlap, changing the transmitter concentration profile in the synaptic cleft. We conclude that the level of postsynaptic receptor occupancy can depend on the probability of transmitter release at individual multi-site synapses.

Electrophysiological studies at the neuromuscular junction (NMJ) have established many of the basic mechanisms that underlie chemically mediated synaptic transmission, including the quantal nature of the release process (Katz, 1969). At central synapses it is also clear that transmitter is released in multimolecular 'packets' or quanta. However, other important features of central transmission, such as the fraction of postsynaptic receptors that bind transmitter and the proportion of channels that open, remain uncertain. These parameters are crucial to our understanding of the mechanisms underlying transmission and plasticity because they link transmitter release with the postsynaptic response.

At the NMJ, postsynaptic receptors are not saturated by transmitter (Hartzell, Kuffler & Yoshikarmi, 1975) and the postsynaptic responses to individual transmitter packets summate in a quantal manner. The postsynaptic responses at a number of central excitatory synapses also appear to behave in a quantal manner, having amplitude histograms with equally spaced peaks (Jack, Redman & Wong, 1981; Larkman, Stratford & Jack, 1991; Kullmann & Nicoll, 1992; Jonas, Major & Sakmann, 1993; Kullmann, 1993; Paulsen & Heggelund, 1994). The low variance of these quantal peaks led to the original proposal that receptors were saturated by transmitter (Jack *et al.* 1981; Redman 1990). More recently, other approaches (Perkel & Nicoll, 1993; Tong & Jahr, 1994) have led to a similar conclusion, implying that the size of the quantal response is determined entirely postsynaptically. However, a number of observations are not consistent with this hypothesis. Several quantal analysis studies found that convincing peaks were apparent only in a subset of cells (Larkman *et al.* 1991; Kullmann & Nicoll, 1992; Jonas *et al.* 1993) and in another study peaks were not apparent (Raastad, Storm & Andersen, 1992). Furthermore, large variability in the postsynaptic response has been observed at synapses where morphological reconstruction indicates the presence of only one synaptic density (Gulyás, Miles, Sík, Tóth, Tamamakl & Freund, 1994) and for miniature excitatory postsynaptic currents (EPSCs) arising from restricted regions of hippocampal cells (Bekkers, Richerson & Stevens, 1990). These results seem incompatible with a model for transmission where the postsynaptic receptors are always saturated. However, complications in the interpretation of amplitude histograms may arise if the size of the quantal response varies between sites or if transmission at synaptic connections is not independent, due to overlap of transmitter released from neighbouring sites (Trussell, Zhang & Raman, 1993) or neighbouring synapses (Faber & Korn, 1988; Tong & Jahr, 1994; Barbour, Keller, Llano & Marty, 1994; Mennerick & Zorumski, 1995).

We have estimated the open probability of the postsynaptic non-*N*-methyl-D-aspartate (non-NMDA) receptors during transmission at the cerebellar mossy fibre–granule cell synapse by analysing current fluctuations at the peak and during the decay of EPSCs. Synapses with a single release site were distinguished from those with multiple release sites by examining the relationship between the probability of transmitter release and EPSC amplitude. Our analyses also provided estimates for the number of channels exposed to transmitter, the fraction of channels occupied by transmitter and the open probability of the transmitter-bound synaptic non-NMDA channels. On the basis of our findings we propose a model for synaptic transmission at the cerebellar mossy fibre–granule cell synapse. Some of these findings have been published in this journal (Silver, Cull-Candy & Takahashi, 1994, 1995) in a preliminary form.

METHODS

Estimation of receptor open probability and occupancy

The open probability of channels at the peak of a ligand-gated membrane current (P_o), is simply the average proportion of channels that are in the open state. This can be calculated for channels with only one open state if the total number of channels exposed to the agonist (N), the single-channel current amplitude (i) and the mean peak current amplitude ($\bar{I}_P$) are known:

$$P_o = \frac{\bar{I}_P}{Ni}. \quad (1)$$

The maximum channel open probability ($P_{o,max}$) occurs when the underlying receptors are saturated by transmitter at the peak of the current. Since not all receptors that bind transmitter will be open at the peak of the current, P_o will be less than the occupancy of the postsynaptic receptors (X). If the channels have a relatively simple receptor reaction scheme (Del Castillo & Katz, 1957) and fast kinetics the receptor occupancy can be calculated from P_o and $P_{o,max}$:

$$X = \frac{P_o}{P_{o,max}}. \quad (2)$$

If the channels require the binding of two (or more) transmitter molecules to open, X will correspond to the occupancy of the doubly bound state provided that access to the open state is permissible only from that state.

For more involved kinetic schemes (e.g. Raman & Trussell, 1992; Jonas *et al.* 1993), estimating occupancy with eqn (2) is not strictly correct. If openings occur from mono- and multi-liganded states, occupancy cannot be defined simply. Complications may also arise for kinetic schemes with desensitized states since $P_o/P_{o,max}$ will give an accurate estimate of occupancy only when the fraction of desensitized receptors is small. This is likely to be true during the rising phase and at the peak of the EPSC but not later during the decay. In some cases $P_{o,max}$ may depend on the *shape* of the transmitter concentration profile. In such cases a change in the shape of the transmitter waveform could change the size of the postsynaptic response without altering the receptor occupancy. This could complicate comparisons of P_o and $P_{o,max}$ at different synapses. We have used the term occupancy throughout, as it is correct for simple kinetic schemes and simulation show that $P_o/P_{o,max}$ predicts the occupancy of the doubly bound states for a modified kinetic scheme of the glutamate receptor GluR-D flip (A. Roth & J. Mosbacher, personal communication). Although this definition of X does not cover the complexities of all possible kinetic schemes it does represent the *fraction of the maximal response*, which is the parameter of physiological importance.

Conventional non-stationary fluctuation analysis of EPSCs

In principle, fluctuations in the amplitude and decay of ion-channel-mediated membrane currents contain information about the number of underlying channels (N) and the single-channel current amplitude (i). N and i can be determined with non-stationary fluctuation analysis (non-SFA) when the underlying channels are independent, homogeneous and have a unitary conductance (Sigworth, 1980). Stochastic channel fluctuations in the decay of the current can be extracted by subtracting the mean (or expectation) current from each individual current. Under these conditions the relationship between the variance of the fluctuations about the mean current (σ^2) and the mean current ($\bar{I}$) is parabolic (Sigworth, 1980):

$$\sigma^2 = i\bar{I} - \frac{\bar{I}^2}{N} + \sigma_B^2. \quad (3)$$

N and i can be determined by fitting the variance–mean current (σ^2–$\bar{I}$) relationship with eqn (3) (where σ_B^2 is the background variance). The σ^2–$\bar{I}$ relationship will be a full parabola (Fig. 1*C*) when all the channels are open at the peak of the current. When the fraction of channels open is low, only the initial, approximately linear, part of the σ^2–$\bar{I}$ plot is obtained (Fig. 1*B*).

Non-SFA has been applied to the sodium current (Sigworth, 1980) and to macroscopic transmitter-gated currents in membrane patches activated by rapid agonist perfusion (Jonas *et al.* 1993; Hestrin, 1992; Spruston, Jonas & Sakmann, 1995). If the underlying channels have multiple conductance states (Wyllie, Traynelis & Cull-Candy, 1993) the σ^2–$\bar{I}$ plot will remain parabolic if the kinetics of the different states are similar and i will correspond to a weighted mean of the currents passing through the different conductance states (Sigworth, 1980). Estimates of the number of channels exposed to transmitter, N, would be overestimated slightly if the channels have multiple conductance states because channel variance will be present even when all the channels are open.

Non-SFA cannot be applied to synaptic currents under most conditions because the population of channels and the channel open probability (P_o) do not remain constant. This is because transmitter release usually occurs from many different sites and transmitter concentration may not be uniform in the cleft. We have overcome these problems by applying non-SFA to EPSCs from inputs with a single synapse at near-physiological temperatures when transmitter release was maximal. Under these conditions the postsynaptic receptors were apparently saturated by transmitter and N and P_o ($P_{o,max}$ in this case) were constant. Of course, it is possible that the mechanisms underlying the decay of synaptic currents could be complicated, with deactivation, desensitization and the transmitter concentration waveform contributing to the decay time course (Barbour *et al.* 1994; Jonas & Spruston, 1994; Silver, Colquhoun, Cull-Candy & Edmonds, 1996*a*). However, non-SFA is not, in principle, dependent on the precise mechanism underlying the fall in channel open probability during the decay of the synaptic current, although it is crucial that the expected waveform of each EPSC is equal to the mean current waveform. The validity of this assumption can be tested by checking that there is no change in the amplitude or decay time course with time and by checking that there are no correlations between the amplitude and decay time of the synaptic currents.

Peak-scaled non-stationary fluctuation analysis of EPSCs

Since conventional non-SFA cannot be applied to synaptic currents under most conditions, we have recently developed a different non-stationary fluctuation analysis method, the peak-scaled non-stationary fluctuation analysis method (Traynelis, Silver & Cull-Candy, 1993). This approach is applicable to a wider range of synaptic currents and has been used to estimate the conductance of synaptic non-NMDA and $GABA_A$ channels in granule cells (Traynelis *et al.* 1993; Brickley, Farrant & Cull-Candy, 1995). This method involves scaling the mean current waveform to the peak of each synaptic current and analysing the variance associated with the closure of channels from the open state. Like conventional non-SFA, peak-scaled non-SFA relies on the assumption that the expected waveform of each individual synaptic current has the same shape as the mean current waveform. However, it differs from conventional non-SFA in that it is independent of variations in N and P_o. It can therefore be applied to inputs where the P_o varies from channel to channel and where the number of channels exposed to transmitter and P_o vary from one current to the next. Peak-scaled non-SFA provides only an estimate of i since information about N and P_o is lost when the mean waveform is scaled to the peak of each current. The relationship between the peak-scaled variance (which is a conditional variance) and the mean current is described by:

$$\sigma_{P\text{-}S}^2 = i\bar{I} - \frac{\bar{I}^2}{N_P} + \sigma_B^2, \quad (4)$$

where $\sigma_{P\text{-}S}^2$ is the peak-scaled variance and N_P is the number of channels *open at the peak* of the synaptic current, *not* the total number of channels exposed to transmitter (Traynelis *et al.* 1993). The $\sigma_{P\text{-}S}^2$–$\bar{I}$ relationship is parabolic when no channels open for the first time after the peak of the EPSC, becoming skewed if channels do open for the first time after the peak. This occurs because channels opening for the first time after the peak create additional variance which distorts the $\sigma_{P\text{-}S}^2$–$\bar{I}$ plot. The weighted mean single-channel current can be estimated by fitting the initial slope of the relationship even when the relationship is skewed (Traynelis *et al.* 1993).

EPSC filtering and non-stationary fluctuation analysis

Non-NMDA channel openings are characteristically brief, raising the possibility that filtering may distort the shape of the EPSCs and thus influence the estimates of the microscopic properties of the underlying channels. The series resistance (R_s), input resistance (R_m) and capacitance (C_m) were measured for each cell from the capacitative current response to a −10 mV voltage step. Electrode-cell parameters were $R_s = 13{\cdot}7 \pm 1{\cdot}7$ MΩ, $R_m = 4{\cdot}2 \pm 1{\cdot}5$ GΩ and $C_m = 3{\cdot}3 \pm 0{\cdot}4$ pF ($n = 11$) at 34 °C and $R_s = 31 \pm 10$ MΩ, $R_m = 30 \pm 25$ GΩ and $C_m = 3{\cdot}3 \pm 0{\cdot}5$ pF ($n = 5$) at 24 °C. The low-pass filtering imposed by the electrode–cell circuit can be directly calculated from these values since modelling of granule cells indicates that the soma and dendrites behave as a single electrical compartment (Silver, Traynelis & Cull-Candy, 1992). Low-pass filtering by the electrode–cell circuit was $4{\cdot}5 \pm 0{\cdot}6$ kHz (range, 2·6–7·9 kHz; −3 dB) at 34 °C and $2{\cdot}5 \pm 0{\cdot}7$ kHz (range, 1·4–5·3 kHz) at 24 °C. This, cascaded with filtering from the amplifier (10 kHz) and apparatus (4·2 kHz), gave a total (approximate) filtering of 3·0 kHz at 34 °C and 2·1 kHz at 24 °C. This corresponds to 10–90% rise times of about 110 and 160 μs, respectively.

Non-SFA of simulated EPSCs illustrated in Fig. 1, indicates that the degree of filtering imposed by the electrode–granule cell circuit and apparatus (see above) has only a small effect on the estimation of i, N and P_o. EPSCs were simulated at 24 and 34 °C with a two-state linear model with rate constants adjusted to mimic non-NMDA channel open times of 600 μs at 24 °C (Wyllie *et al.* 1993) and 350 μs at 32 °C (estimated from channel deactivation: Silver *et al.* 1996*a*). The association and dissociation rate constants used

were $k_{+1} = 1{\cdot}6 \times 10^6$ M^{-1} s^{-1} and $k_{-1} = 1{\cdot}67 \times 10^3$ s^{-1} for 24 °C and $k_{+1} = 3 \times 10^6$ M^{-1} s^{-1} and $k_{-1} = 2{\cdot}86 \times 10^3$ s^{-1} for 34 °C. The channels ($N = 180$–500) had a 12 pS open state and were activated with a 0·1 ms square pulse of transmitter. Runs of 1000–2000 simulated EPSCs with different P_o values were generated by altering the concentration of transmitter: at 24 °C, 1 mM transmitter gave a P_o of 0·145 and 14 mM gave a P_o of 0·85, while at 34 °C, 0·6 mM gave a P_o of 0·158 and 9 mM gave a P_o of 0·86. Filtering was imposed with a digital Gaussian filter (Traynelis *et al.* 1993). Panels *A–C* and *D–F* in Fig. 1 show the effect of filtering encountered during recordings at 24 and 34 °C, respectively, on the simulated EPSCs and non-SFA. Even the heaviest filtering encountered did not alter the shape of low- or high-P_o σ^2–$\bar{I}$ relationships. The mean level of filtering encountered during recordings (2·1 kHz at 24 °C and 3 kHz at 34 °C) had little effect on the estimated channel conductance (93 and 95%), on N (96 and 97%) or on P_o (98 and 98%). Even in the worst cases (1·33 kHz at 24 °C and 2·2 kHz at 34 °C) the effects on the estimated channel conductance (90 and 88%), N (89 and 104%) and P_o (93 and 92%) were still relatively small. These results suggest that in the granule cell filtering is unlikely to distort seriously estimates of i and N or P_o.

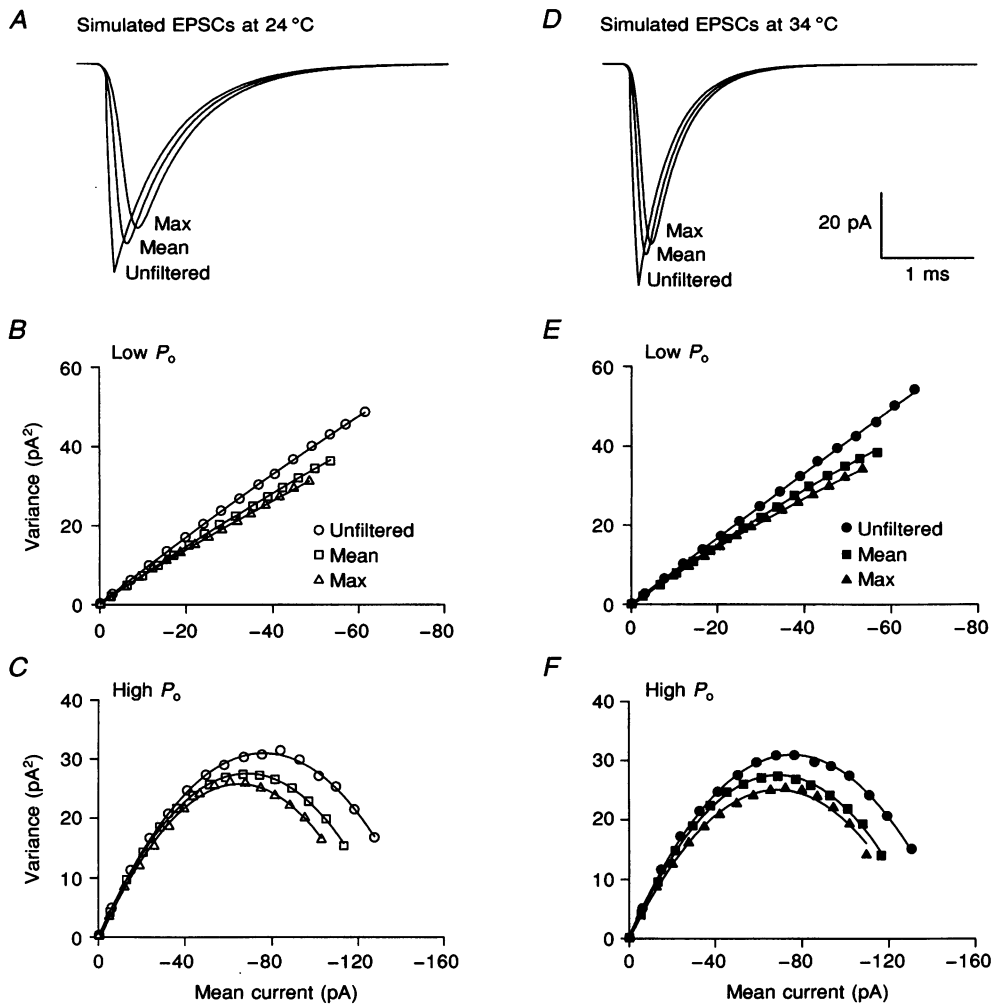

Figure 1. The effect of filtering on non-stationary fluctuation analysis of synaptic currents

A–C, analysis of simulated EPSCs that mimic the mossy fibre–granule cell synaptic current at 24 °C. *A*, averages of 2000 simEPSCs with zero (Unfiltered), 2·1 kHz (Mean) and 1·33 kHz (Max) filtering imposed. *B*, variance–mean current plots (σ^2–$\bar{I}$) from non-SFA of simulated EPSCs under the same filtering conditions as *A* for a glutamate concentration that gave a low channel open probability ($P_o = 0{\cdot}145$). *C*, σ^2–$\bar{I}$ plots from non-SFA of simulated EPSCs under similar filtering conditions for a glutamate concentration that gave a high channel open probability ($P_o = 0{\cdot}85$). *D–F*, analysis of simulated EPSCs that mimic the mossy fibre–granule cell synaptic current at 34 °C. *D*, averages of 2000 simulated EPSCs with zero (Unfiltered), 3 kHz (Mean) and 2·2 kHz (Max) filtering imposed. *E*, variance–mean current plots (σ^2–$\bar{I}$) from non-SFA of simulated EPSCs under similar filtering conditions to *D* for a glutamate concentration that gave a low channel open probability ($P_o = 0{\cdot}158$). *F*, σ^2–$\bar{I}$ plots from non-SFA of simulated EPSCs under similar filtering conditions for a glutamate concentration that gave a high channel open probability ($P_o = 0{\cdot}86$). These simulations indicate that the levels of filtering encountered during recording had only a small effect on estimates of i and N (see Methods).

Electrophysiological recordings from cerebellar slices

Following decapitation, the brains from 10- to 14-day-old rats were removed and cooled in ice-cold saline for approximately 1 min. Wistar rats were used throughout, with the exception of those experiments shown in Fig. 2*C* where Sprague–Dawley rats were used. Parasagittal slices of cerebellum (150 μm thick) were cut (Edwards, Konnerth, Sakmann & Takahashi, 1989) with a microslicer (DTK-1000, D.S.K, Dosaka EM Co., Ltd, Japan). Slices were then incubated at 31 °C for 1 h. The saline solution used for slicing and incubation contained (mM): 125 NaCl, 2·5 KCl, 1 $CaCl_2$, 5 $MgCl_2$, 1·25 NaH_2PO_4, 26 $NaHCO_3$, 15 lactate and 15 glucose (pH 7·3 when bubbled with 95% O_2 and 5% CO_2). Slices were then transferred to the recording chamber which was perfused with external solutions containing (mM): 125 NaCl, 2·5 KCl, 0·5–2 $CaCl_2$, 1–5 $MgCl_2$, 1·25 NaH_2PO_4, 26 $NaHCO_3$ and 15 glucose (pH 7·3 when bubbled with 95% O_2 and 5% CO_2). Recordings of the non-NMDA receptor component of the EPSC were made at 24 °C (23–25 °C) and 34 °C (32–37 °C) with 20 μM D-amino-5-phosphonopentanoic acid, 20 μM 7-chlorokynurenic acid and 15 μM bicuculline methiodide added to the perfusate to block NMDA and γ-aminobutyric acid receptors, respectively. In a few experiments 4-phorbol-1,13-dibutyrate (1 μM) was added in an attempt to increase the release probability but it had no effect. Patch pipettes (5–15 MΩ) were made from thick-walled borosilicate glass (Clark Electromedical, Reading, UK) and coated with Sylgard (Dow Corning). The pipette solution consisted of (mM): 110 CsF, 30 CsCl, 4 NaCl, 0·5 $CaCl_2$, 10 Hepes and 5 EGTA (pH 7·3). Mossy fibre inputs were stimulated at 0·2–1 Hz (5–20 V, duration 200 μs) with a second patch electrode filled with 1 M NaCl placed on the surface of the surrounding tissue (Fig. 2*A* and *B*). EPSCs were recorded using an L/M-EPC-7 amplifier (List) and recorded on videotape (RP-880; NF-Electronic Instruments) and digitized at 70–100 kHz (pCLAMP 5.5; Axon Instruments). All values are expressed as means ± S.E.M. except where specified. Amplitude distributions were fitted with Gaussian functions using the maximum likelihood method (EKDIST; Colquhoun & Sigworth, 1995). Different measurements were compared with either Student's *t* test, the Spearman rank-order correlation test, or the Kolmogorov–Smirnov test (Press, Teukolsky, Vetterling & Flannery, 1994) and considered significant at the $P < 0.05$ level.

Practical aspects of the analysis of synaptic currents

EPSCs were distinguished from the noise by eye. In those cases where the noise level prevented unambiguous identification of EPSCs the trace was digitally filtered to improve resolution. However, there was usually a good separation between the EPSC and the background noise (S.D. = 1·53 ± 0·06 pA, $n = 5$ at 24 °C and S.D. = 1·87 ± 0·08 pA, $n = 9$ at 34 °C for an applied level of filtering of 4·2 kHz, −3 dB), even for the smallest events (see Fig. 6). Those trials with a high noise level due to 'membrane breakdown' were omitted. All trials without EPSCs were considered failures. Stable stretches of consecutive EPSCs were identified for non-SFA by checking the amplitude and decay time course for stability (see Fig. 3*B*) using the Spearman rank-order correlation test. Groups of consecutive EPSCs that had no significant relationships between amplitude and 62% decay time and between amplitude and 10–90% rise time (Fig. 3*C*) were used for analysis. Since single-site EPSCs were made up of only a few channels and their waveform was, proportionately, more affected by background noise, we used only the stability of amplitude and decay time courses as criteria for selecting epochs suitable for analysis (see Fig. 8*A*).

Non-SFA was carried out in a manner similar to that previously described (Sigworth, 1980; Traynelis *et al.* 1993). Briefly, EPSCs were averaged by aligning on their rising phase. The average EPSC waveform was then subtracted from individual EPSCs and the variance of the fluctuations around the mean current was calculated for 10–100 bins. Each bin had an equal current decrement (the duration of the time window was determined by the average current decay time course) giving, on average, the same number of channel closures. The variance for each bin was averaged over all the EPSCs in the epoch and plotted against mean current. The relationship between variance and mean current was fitted with eqn (3) to determine N and i. Channel conductance was calculated with measured EPSC reversal potentials at 24 °C (Fig. 2*C*) and 34 °C; since the measured liquid junction potential was small (3 mV) no correction was made. Peak-scaled non-SFA was carried out in a similar manner except that the mean EPSC waveform was scaled to the peak of each individual EPSC before subtraction. The peak-scaled variance–mean current plot was fitted with eqn (4) to determine i and N_P. If the $\sigma^2_{P\text{-}S}$–$\bar{I}$ relationship was skewed only the initial part of the plot was fitted to give i and N_P was calculated from $\bar{I}_P/i$. The peak amplitudes of EPSCs were estimated by averaging the three digitized points at the peak of the current. When the amplitudes of the largest individual single-site EPSCs (I_{max}; Fig. 9*C*) were measured, cells that had a lower signal-to-noise ratio were digitally filtered to 2–2·5 kHz in order to reduce the distortion of peak amplitude by background noise.

For the experiments in which the synaptic current waveforms were compared at different release probabilities (Figs 11 and 12), the EPSCs were averaged by aligning on the stimulus artifact so that the average EPSC waveform included asynchrony of transmitter release. The decay time course was fitted with the sum of two exponential functions with the baseline fixed. Since the slow exponential component of the EPSC was small and variable the decay time constant of the fast component was used for comparison. The temperature dependence of the standard deviation of the EPSC latency distribution was calculated with a temperature coefficient, Q_{10}, of (latency S.D. at T_1/ latency S.D. at T_2)$^{10/(T_2 - T_1)}$, where T_1 is the lower and T_2 is the higher temperature.

Modelling transmitter release

In order to identify synapses with a single release site it was necessary to determine the relationship between the proportion of transmission failures, f, and the postsynaptic responses of synapses with different numbers of release sites. These relationships were derived assuming that release was independent, that a release site released a maximum of one quantum per action potential (Redman, 1990; Korn & Faber, 1991), and that the postsynaptic responses summated linearly. Initially, it was assumed that the release probability and the mean quantal size were uniform across release sites. The release probability at each site (P_r) could therefore be calculated from f. The change in the EPSC amplitude was expressed as the ratio of expected EPSC amplitudes during low (low $[Ca^{2+}]/[Mg^{2+}]$, L: 0·5–1·25 mM/3–5 mM) and high (normal $[Ca^{2+}]/[Mg^{2+}]$, N: 2 mM/1 mM) release probability conditions (b/a in Fig. 5*B*). Under these conditions the relationship between b/a and f observed in the different $[Ca^{2+}]/[Mg^{2+}]$ solutions is given by:

$$\frac{b}{a} = \left(\frac{1 - f_L^{1/n}}{1 - f_N^{1/n}}\right)\left(\frac{1 - f_N}{1 - f_L}\right), \quad (5)$$

where n is the number of release sites and f_L and f_N are the

proportion of failures in low and normal $[Ca^{2+}]/[Mg^{2+}]$ conditions (see Fig. 5*C*). The smallest change in b/a for multi-site synapses occurred at synapses with only two release sites.

We extended this approach by developing the 'worst case' two-site model in which release probability and postsynaptic response were not the same at both sites. If the ratio of the probability of release at the two sites is similar in normal and low $[Ca^{2+}]/[Mg^{2+}]$ solutions, b/a becomes independent of differences in the quantal size at the two sites. b/a can therefore be expressed in terms of the proportion of release (R) at one site ($R = P_{r1}/(P_{r1} + P_{r2})$) and the fraction of failures:

$$\frac{b}{a} = \left(\frac{1 - \sqrt{(1 - 4R(1 - R)(1 - f_L))}}{1 - \sqrt{(1 - 4R(1 - R)(1 - f_N))}}\right)\left(\frac{1 - f_N}{1 - f_L}\right). \quad (6)$$

This is equivalent to the model above when release at the two sites is equal ($P_{r1}/(P_{r1} + P_{r2}) = 0{\cdot}5$). The sensitivity of using the lack of dependence of b/a on f as an indicator of single-site synapses is highly dependent on the change in f between the high and low probability conditions (see Fig. 5*D*). We have therefore only used inputs with an $f \leqslant 0{\cdot}3$ for the high release conditions. Synaptic inputs were considered to have only a single release site when the observed b/a value was closer to 1 than the predicted b/a values over the range $0{\cdot}15 < P_{r1}/(P_{r1} + P_{r2}) < 0{\cdot}85$ for the observed change in failure rate.

Diffusion calculations

In order to determine whether overlap of transmitter from neighbouring sites was feasible, we calculated whether sufficient time was available for glutamate to diffuse between sites. Since many of the factors that will determine the rate of diffusion in the cleft remain unknown, this approach can only give an approximate estimate. Diffusion away from the release site was modelled with a line source in an infinite volume. For such a case (Crank, 1975) the concentration of transmitter ($C(t)$) at a distance r from the release site is described by:

$$C(t) = (M/4\pi Dt)\exp(-r^2/4Dt), \quad (7)$$

where M is the amount of substance per unit length of the line source (which is related to the amount of transmitter released per site), D is the diffusion coefficient and t is time. The distance r was

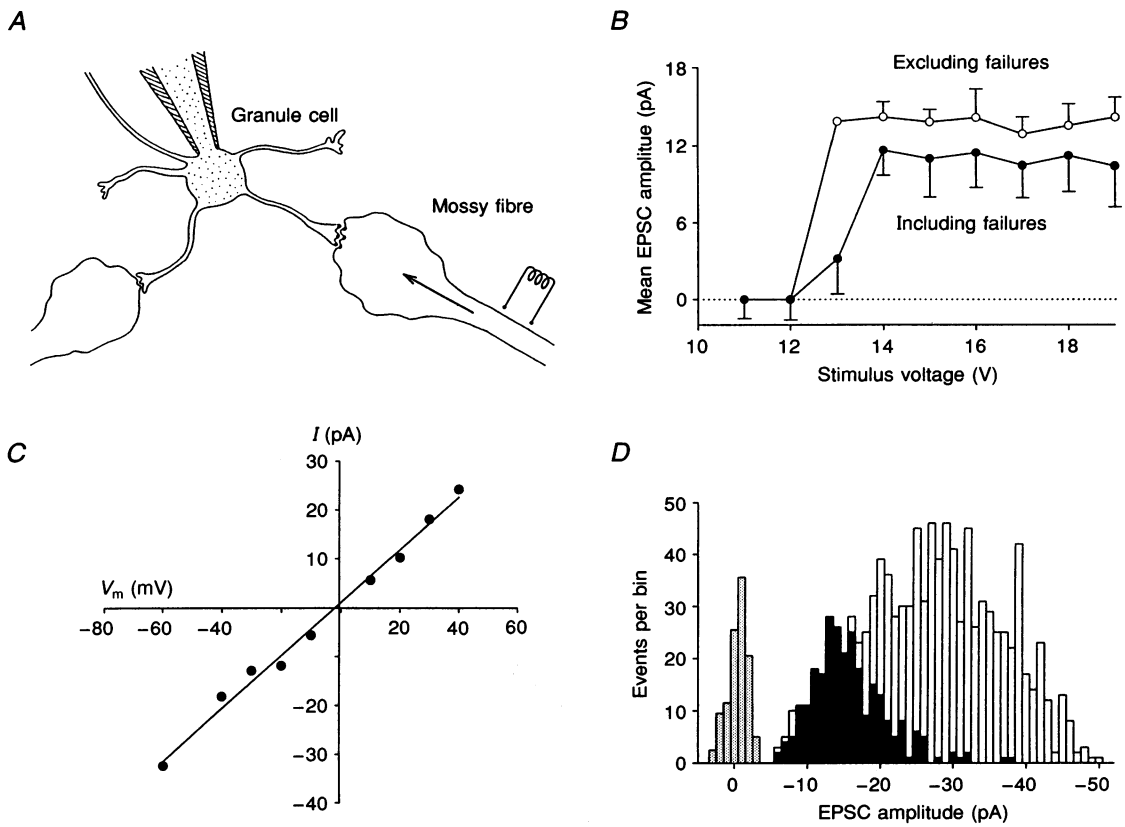

Figure 2. General properties of the cerebellar mossy fibre–granule cell synapse

A, schematic diagram of synaptic morphology and whole-cell patch-clamp recording. The coil represents a stimulating electrode and the hatched area corresponds to the patch pipette. *B*, relationship between mean EPSC amplitude and applied stimulus voltage for a putative single mossy fibre input. ○, mean EPSC amplitude, averaged on the rising phase of the EPSC and excluding failures. The error bars show the S.E.M.; the lower limbs were omitted for clarity. Only 2 EPSCs occurred at 13 V so no error bars are shown. ●, mean EPSC amplitude including failures. The upper limbs of the standard error bars were omitted for clarity. *C*, synaptic current–voltage relationship; each point represents the average of 10–20 EPSCs. The data were well fitted by a linear relationship (continuous line). *D*, EPSC amplitude histograms recorded at −80 mV in 2 mM Ca^{2+} and 1 mM Mg^{2+} (open columns, 993 events; proportion of transmission failures, $f = 0{\cdot}009$) and 0·5 mM Ca^{2+} and 5 mM Mg^{2+} (black, 265 events; $f = 0{\cdot}77$) with background noise (grey, 220 events scaled by 0·5).

set at 0·7 μm since serial section electron microscopy indicates that the average distance between release sites is about 0·6–0·7 μm at the mossy fibre–granule cell synapse (Hámori & Somogyi, 1983). The diffusion coefficient for glutamate was assumed to be equal to that for glutamine in free solution, which was $D = 1 \times 10^{-5}$ cm^2 s^{-1} when corrected for temperature (35 °C). These parameters indicate that the peak of the transmitter concentration would occur at the neighbouring site in about 120 μs. It should be noted that this estimate is likely to represent a lower limit for the diffusion time from one density to the next, since structures in the cleft and non-planar cleft geometry will tend to retard the diffusion rate.

RESULTS

Single mossy fibre inputs

Granule cells are small (soma diameter, ~7 μm) with, on average, four short (~13 μm) largely unbranched dendrites. Each dendrite terminates in finger-like processes called digits which are short and stubby at postnatal day 12 (Hámori & Somogyi, 1983). This compact morphology, allows voltage-clamp recordings of exceptional resolution (Silver *et al.* 1992).

The electrotonic structure of granule cells has been investigated both experimentally and with digital models based on anatomical and electrical measurements from whole-cell recordings (Silver *et al.* 1992; Silver, Farrant & Cull-Candy, 1996*b*). These studies indicate that the soma and dendrites of the granule cell have a small capacitance (~3·3 pF) and behave as a single electrical compartment. Direct measurement of synaptic filtering by the electrode–cell circuit shows that filtering of the synaptic current is very light (Silver *et al.* 1996*b*; see Fig. 1 and Methods). Indeed, the low background noise and excellent quality of voltage clamp allows resolution of individual synaptic NMDA (Silver *et al.* 1992) and $GABA_A$ (Brickley *et al.* 1995) channels in excitatory and inhibitory synaptic currents.

As depicted in Fig. 2*A*, the excitatory synaptic arrangement onto granule cells is simple, with each dendrite receiving innervation from a different mossy fibre input (Eccles, Ito & Szentagothai, 1967). The small number of synapses onto the

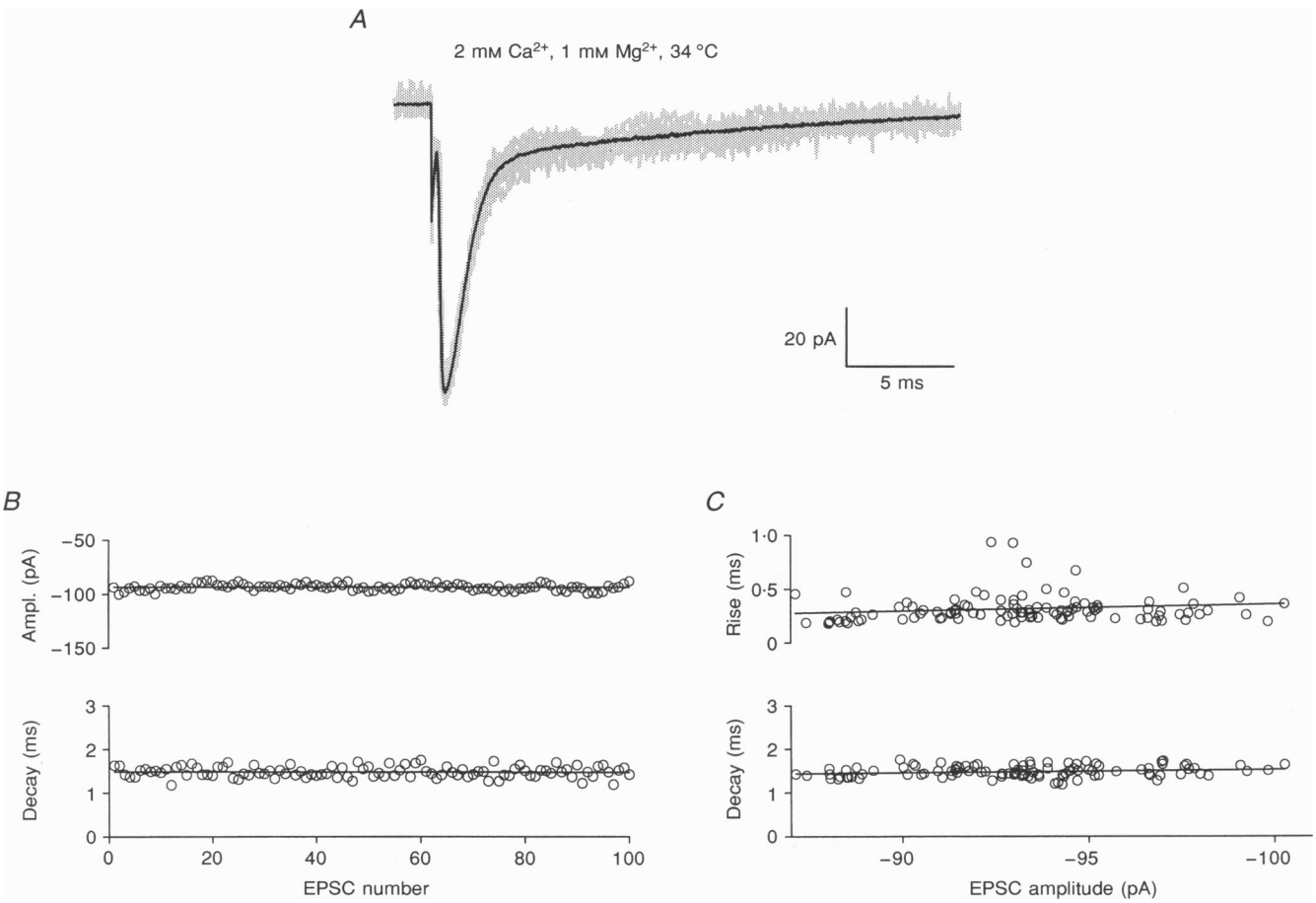

Figure 3. Stability of invariant EPSCs from a multi-site synapse at 34 °C

A, EPSCs from a mossy fibre input that exhibited little variation in peak amplitude at 34 °C. Grey lines are 10 superimposed individual EPSCs recorded at −70 mV in 2 mM Ca^{2+} and 1 mM Mg^{2+}; black line shows the average of 104 EPSCs. *B* shows the peak amplitude and decay time (to 62% of peak amplitude) of sequential EPSCs in the epoch. Regression analysis (continuous line) indicated that both amplitude and decay were stable during the epoch. *C* shows the relationship between EPSC rise time (10–90%) and peak amplitude and EPSC decay time (62%) and peak amplitude. There was no significant correlation between these parameters.

granule cell (~4) and the diffuse network of mossy fibres in the granule cell layer (mossy fibres run in fibre tracts until they enter the granule cell layer; Palay & Chan-Palay, 1974) permitted the activation of single mossy fibre synapses with an electrode placed in the surrounding tissue. Single mossy fibre inputs were identified by the all-or-none appearance of EPSCs in response to a stimulus of graded intensity (Takahashi, 1992) as illustrated in Fig. 2*B*. The current–voltage relationship of the non-NMDA component EPSCs was linear (Fig. 2*C*). This linearity was also obtained when 100 μM spermine was added to the internal solution ($n = 5$; data not shown) suggesting that the synaptic non-NMDA receptors were of the Ca^{2+}-impermeable subtype (see Kamboj, Swanson & Cull-Candy, 1995; Koh, Burnashev & Jonas, 1995). The EPSC peak amplitude fluctuated over a wide range (Fig. 2*D*, open columns) but did not exhibit clear peaks. When the release probability was lowered by reducing $[Ca^{2+}]$ to 0·5 mM and increasing $[Mg^{2+}]$ to 5 mM, the variability and size of such responses were reduced (Fig. 2*D*; black columns), suggesting that these EPSCs resulted from the release of multiple packets of transmitter.

Transmission at synapses with multiple release sites

At 32–37 °C the peak amplitude of EPSCs (1330 ± 280 pS, $n = 5$) arising from some of these inputs was remarkably invariant (Fig. 3*A*), raising the possibility that the non-NMDA receptors were saturated by the neurotransmitter glutamate. Non-stationary fluctuation analysis (Sigworth, 1980) was applied to sets of such invariant EPSCs where the peak amplitude and decay time course were stable (Fig. 3*B*) and the rise time and decay were not correlated with peak amplitude (Fig. 3*C*). Some of these inputs had an almost complete parabolic relationship between the variance of the decay and the mean current (Fig. 4*A*), indicating that most of the postsynaptic channels were open at the peak of the EPSC.

It is unlikely that the $\sigma^2 - \bar{I}$ relationship shown in Fig. 4*A* arises from variations in the transmitter concentration waveform rather than the stochastic gating of postsynaptic channels for the following reasons. (1) If variance arose from variations in transmitter concentration it would be expected to be greatest at the peak of the current. (2) All of the variance observed at these high P_o inputs (and its relationship to the mean current), could be accounted for by the stochastic gating of postsynaptic non-NMDA channels. (3) The estimated channel conductance was independent of changes in the mechanisms underlying the EPSC decay. Peak-scaled non-SFA (see Methods) of EPSCs recorded from the same multi-site synaptic input under high and low release probability conditions gave similar estimates for channel conductance even though the EPSC decay rate was different under the two conditions (Fig. 11). (4) Our estimates for the non-NMDA channel conductance are within the range of conductances reported for non-NMDA channels in patches (Hestrin, 1992; Jonas *et al.* 1993; Wyllie *et al.* 1993; Spruston *et al.* 1995). (5) No correlation was observed between either decay time course and peak amplitude or rise time and peak amplitude (Fig. 3*B* and *C*).

The high proportion of channels open is consistent with the presence of a saturating concentration of transmitter in the synaptic cleft (see Methods). The EPSC amplitude distributions of these inputs (illustrated in Fig. 4*B*) also suggested that the postsynaptic receptors were saturated by transmitter, having a narrow Gaussian shape and a coefficient of variation (c.v. = standard deviation/mean

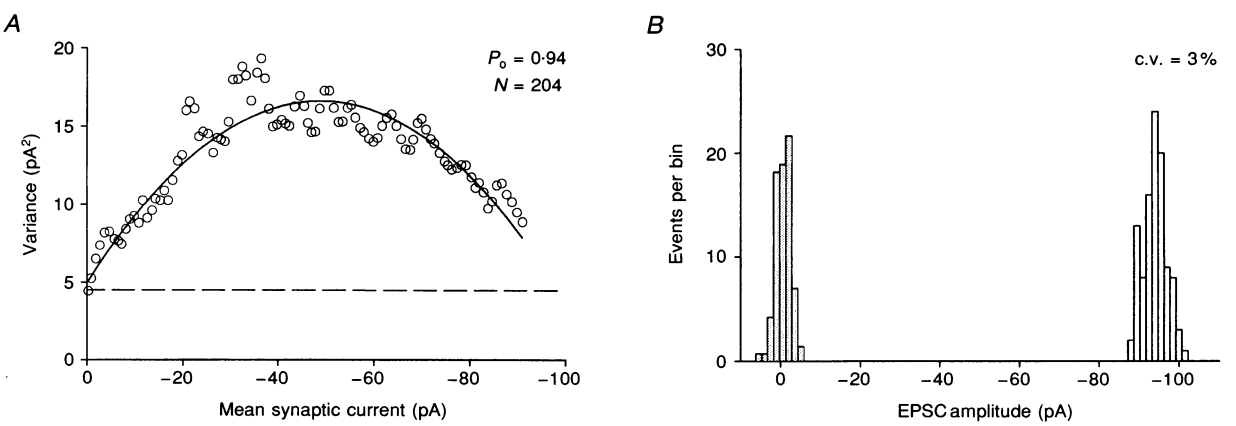

Figure 4. High open probability of postsynaptic non-NMDA channels during synaptic transmission at a multi-site synapse

A, variance–mean current relationship from conventional non-stationary fluctuation analysis of the EPSCs shown in Fig. 3. Fluctuations in the decay of EPSCs were analysed by subtracting the mean waveform from each EPSC. The decay was divided into 100 bins and variance and mean current was calculated for each bin. The plot of variance against mean current was fitted with eqn (3) (continuous line) to give the total number of channels exposed to transmitter, N, and the mean single-channel current, i. This gave estimates of $N = 204$ and $i = 0{\cdot}48$ pA for this synapse. The parabolic shape of the relationship indicates that almost all of the channels are open at the peak of the current and that the open probability of the synaptic non-NMDA channels at the peak of the EPSC, P_o, is high. The dashed line indicates the baseline variance. *B*, EPSC peak amplitude histogram from the same cell (open columns) with associated background noise (shaded columns). c.v. is the coefficient of variation (background noise corrected).

current) of only 0·04 ± 0·01 (corrected for background noise). Since the non-SFA method was only applicable to synapses where the postsynaptic receptors were saturated by transmitter (see Methods), we used the five synapses with the highest channel open probability at the peak of the EPSC for our analysis. At these synapses the open probability of the synaptic non-NMDA channels (P_o) was 0·84 ± 0·03 (range, 0·74–0·94). Under these conditions P_o will be equal to the open probability of the channel when bound by transmitter ($P_{o,max}$).

If the postsynaptic receptors were not fully saturated, fluctuations in the amount of transmitter in the cleft (arising from variation in the vesicle size and number of vesicles released) would alter the size of the EPSC and increase the variance. We have tested whether the postsynaptic receptors are saturated by transmitter by comparing the number of channels open at the peak, determined from conventional non-SFA (140 ± 30; this will include variance arising from any variations in transmitter concentration), and from peak-scaled non-SFA (140 ± 30; this method excludes variance arising from variations in transmitter concentration). The fact that these two different methods gave the same estimates for the number of channels open at the peak indicates that the variance arising from fluctuations in transmitter concentration was negligible, that P_o was constant from one EPSC to the next and that the postsynaptic channels were exposed to a saturating concentration of glutamate at these inputs.

The initial slope of the σ^2–$\bar{I}$ relationship gave an estimate of the weighted mean single-channel current for the non-NMDA channels underlying the EPSCs (this gave a conductance of 10 ± 1 pS, $n = 5$, at 34 °C). Extrapolation of the fit of eqn (3) to the data gave an estimate of 170 ± 40 (range, 64–307) for the number of non-NMDA channels exposed to transmitter at the peak of the EPSC.

If the synaptic non-NMDA channels had multiple conductance levels, channel variance would still be present when all of the channels were open. However, even if all the variance at the peak of the EPSC arose from this, N would be overestimated by only 20% because extrapolation of the fit of eqn (3) was 20% greater than the mean number of channels open at the peak of the EPSC.

The amplitude of these 'saturating' EPSCs was reduced by lowering $[Ca^{2+}]$ and raising $[Mg^{2+}]$, indicating that they arose from the release of multiple packets of transmitter (see Fig. 11*A*). Saturation of the postsynaptic receptors at these multi-site synapses could occur by linear summation of independent sites, each saturated by a single packet of transmitter, although each release site would have to have a release probability of 1. Alternatively, saturation could occur by summation of transmitter concentration within the synaptic cleft. We investigated which of these mechanisms underlies transmission at these mossy fibre–granule cell synapse.

Identification of synapses with a single release site

Serial section electronmicroscopy has indicated that few synaptic densities are present at each mossy fibre–granule cell synapse (3 on average; Jakab & Hámori, 1988). In some of our recordings, evoked EPSCs were comparable in size to spontaneous miniature EPSCs (Silver *et al.* 1992), raising the possibility they might arise from a synapse with a single release site. If a nerve impulse releases a maximum of one packet of transmitter per site (Redman, 1990; Korn & Faber, 1991), release at synapses with one site will be 'all-or-nothing'. Changes in the release probability will simply alter the proportion of transmission failures (f) rather than the size of the mono-quantal EPSCs. In contrast, lowering the release probability at a synapse with multiple release sites is expected to reduce the average number of quanta per EPSC and therefore reduce the size of the EPSCs. We have used this difference in behaviour to identify synapses with a single functional release site. The probability of release was manipulated by altering the $[Ca^{2+}]/[Mg^{2+}]$ ratio and determined from f.

Figure 5*A* shows averaged EPSCs recorded from a cell in two different $[Ca^{2+}]/[Mg^{2+}]$ solutions that gave different probabilities of transmitter release. When the release probability was substantially reduced (as judged from f) the mean EPSC amplitude (excluding failures) did not change, suggesting that this synapse had only one release site. In contrast, lowering the release probability at a synapse with multiple release sites reduced the EPSC amplitude as shown in Figs 2*D*, 5*B* and 10*A*. The fact that the EPSCs in Fig. 5*B* are of similar size and were recorded under similar conditions to those from the single-site synapse in Fig. 5*A* illustrates that EPSCs close to the mean quantal size can arise from multi-site synapses. Thus single-site synapses cannot be identified on EPSC size alone.

Possible presynaptic mechanisms for EPSC failure include (i) stochastic failure of transmitter release, (ii) action potential failure (at a branch point) and (iii) events missed due to background noise. However, several lines of evidence suggest that the changes in f that we observe are due to stochastic failure of transmitter release. Calcium and magnesium have opposite effects on transmitter release (Katz, 1969; Kuno & Takahashi, 1986), but both have a stabilizing effect on cell excitability, with $[Ca^{2+}]$ being about twice as effective as $[Mg^{2+}]$ (Frankenhaeuser & Hodgkin, 1957). By lowering the $[Ca^{2+}]$ and raising the $[Mg^{2+}]$ we would expect to maintain a similar level of neuronal excitability and reliable action potential invasion (see Kuno & Takahashi, 1986). Moreover, branch point failure is unlikely to occur in the area of stimulation (200 μm radius) because once mossy fibres enter the granule cell layer they exhibit relatively little branching (Palay & Chan-Palay, 1974). The exceptional quality of the voltage clamp and the low membrane noise present in granule cells makes the separation of failures from EPSCs much more reliable than for larger neurones (see Fig. 6). Thus, for granule cells under our conditions it seems likely that changes in f reflect changes in presynaptic release probability rather than these other possible mechanisms.

The relatively small changes in $[Ca^{2+}]$ (2–0·5 mM) and $[Mg^{2+}]$ (1–5 mM) that were used to alter P_r did not change the estimated channel conductance ($P > 0·05$, $n = 5$). This is consistent with the linear current–voltage relationship (Fig. 1*B*) and the presence of mRNA for the GluR-2 glutamate receptor subunits, both of which suggest that the synaptic channels are relatively calcium impermeable (Seeburg, 1993; Hollmann & Heinemann, 1994).

In order to establish quantitative criteria for identifying synapses with only one functional release site we have modelled the behaviour of synapses with different numbers of release sites. A single release site was defined functionally as a site that released one packet of transmitter with a probability P_r. The amount of transmitter per packet could vary, but the mean transmitter content was stable with time and was independent of P_r. The ratio of expected EPSC amplitudes at low and high release probabilities (equivalent to b/a in Fig. 5*B*) was calculated from the proportion of failures observed in different $[Ca^{2+}]/[Mg^{2+}]$ solutions. Since the size of the expected reduction in EPSC amplitude was strongly dependent on the change in f, only those inputs with an intrinsically low failure rate ($f \leqslant 0{\cdot}3$) could be used. Figure 5*C* shows the expected fractional EPSC amplitude, for a given change in f (from 0·15 to 0·8), at synapses with different numbers of sites. The expected reduction in EPSC amplitude becomes more pronounced as the number of release sites is increased. Ideally, no change in the size of the EPSC is expected as the release probability is lowered at single-site synapses. However, in practice, small changes are likely to occur due to sampling errors, changes in ambient glutamate or loss of receptors due to rundown.

Modelling release shows that it is most difficult to discriminate between synapses with a single release site and synapses with two sites. We therefore developed the two-site model further to include different probabilities of

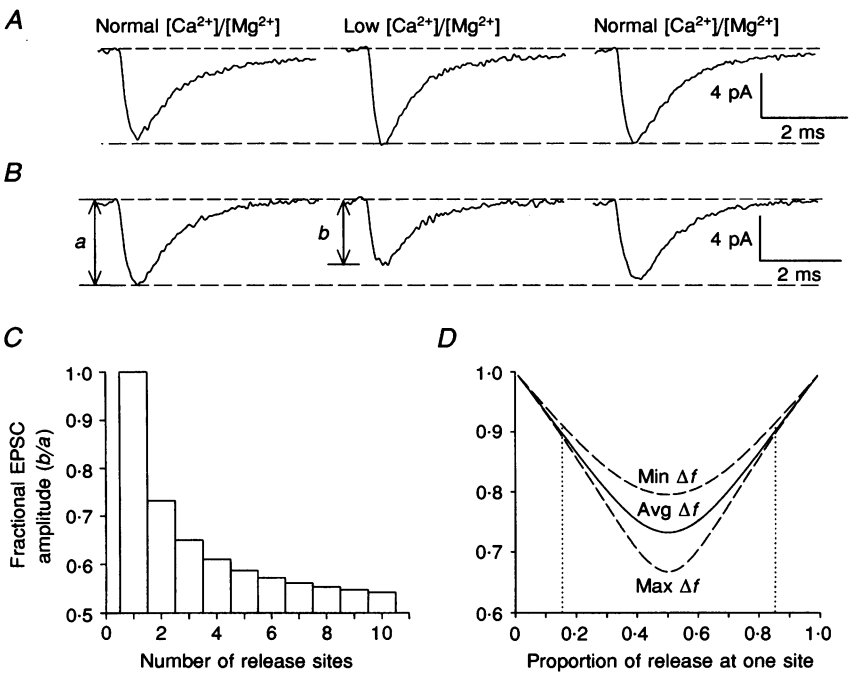

Figure 5. Identification of synapses with a single functional release site

A, 3 averaged EPSCs (means of 180, 167 and 284 EPSCs; excluding failures) recorded from a synapse in two solutions containing different Ca^{2+} and Mg^{2+} concentrations (normal $[Ca^{2+}]/[Mg^{2+}]$: 2 mM/1 mM; low $[Ca^{2+}]/[Mg^{2+}]$: 0·875 mM/4 mM) at 25 °C. The fraction of failures was 0·18, 0·72 and 0·08, respectively. The similarity of the EPSC amplitudes in the different $[Ca^{2+}]/[Mg^{2+}]$ solutions suggested that this synapse had only a single release site. *B*, 3 averaged EPSCs from a different synapse (means of 208, 94 and 220 EPSCs) recorded under similar conditions. The fraction of failures was 0·14, 0·84 and 0·27, respectively. a indicates the peak EPSC amplitude in normal $[Ca^{2+}]/[Mg^{2+}]$ solution and b indicates the EPSC peak amplitude in low $[Ca^{2+}]/[Mg^{2+}]$ solution. The mean EPSC amplitude fell by 22% when recorded in the low $[Ca^{2+}]/[Mg^{2+}]$ conditions suggesting that this synapse had more than one release site. *C*, the expected relationship (from eqn (5)) between the ratio of the EPSC amplitudes at low and high probabilities of release (b/a in *B*) and the number of release sites present at the synapse. Changes in the postsynaptic response were calculated from the proportion of failures in normal ($f_N = 0{\cdot}15$) and low ($f_L = 0{\cdot}8$) $[Ca^{2+}]/[Mg^{2+}]$ solutions. The smallest change in b/a for multi-site synapses occurred at synapses with only two release sites. *D*, a two-site model in which release probability and postsynaptic response were not the same at both sites (eqn (6)). The continuous line marked 'Avg Δf' shows b/a as a function of the proportion of release at one site, $P_{r1}/(P_{r1} + P_{r2})$, for typical values of f_L and f_N as in *C*. The dashed lines marked 'Max Δf' and 'Min Δf' indicate the expected relationship for the largest and the smallest change in failure rate we observed experimentally for a putative single-site synapse ($f_L = 0{\cdot}7$ and $f_N = 0{\cdot}05$ and $f_L = 0{\cdot}89$ and $f_N = 0{\cdot}3$, respectively). The dashed lines show the criterion for the identification of single sites in terms of $P_{r1}/(P_{r1} + P_{r2})$.

release at the two sites. Predictions from this model are illustrated in Fig. 5*D* and show that the expected reduction in the EPSC becomes smaller as the P_r values of the two release sites diverge. This is because the 'effective' number of release sites approaches one. If the ratio of the P_r values at the two sites are similar under the different Ca^{2+} and Mg^{2+} conditions, the fractional change in the EPSC is independent of the quantal size at each site. We have used this two-site model to set our criterion for identifying single-site synapses. The identification threshold for b/a was calculated from the proportion of release at one site, $P_{r1}/(P_{r1} + P_{r2})$, and from the value for f observed during conditions of high and low release probability (since this is more informative than choosing an arbitrary reduction in EPSC amplitude). If a probability range $0{\cdot}15 < P_{r1}/(P_{r1} + P_{r2}) < 0{\cdot}85$ is used (Fig. 5*D*) then five cells (out of 29 with an initial value for $f \leqslant 0{\cdot}3$) exhibited a smaller change in b/a than that predicted from the model. These inputs were therefore considered to be single-site synapses. Inputs identified with this approach are likely to have only one release site, although it should be noted that the presence of additional release sites with low release probabilities (proportion of release at the site with the lowest release probability would be < 15%) cannot be ruled out.

Transmission at synapses with one release site

Analysis of EPSCs from synapses with one release site has allowed us to determine several parameters that are difficult to ascertain from multi-site or multiple synaptic preparations. The probability of release at the five identified putative single-site synapses was $0{\cdot}85 \pm 0{\cdot}04$ (range, 0·7–0·95) in a normal $[Ca^{2+}]/[Mg^{2+}]$ solution at 24 °C. Mossy fibre inputs with failure rates higher than that necessary for the method of identification of single-site synapses ($f > 0{\cdot}3$) were also observed in normal $[Ca^{2+}]/[Mg^{2+}]$ solution, indicating that P_r was lower than 0·7 at the release site(s) of these synapses. Figure 6*A* shows examples of individual EPSCs from an identified single-site synapse. The mean amplitude of EPSCs (excluding failures) from five single-site synapses ranged from 8 to 14 pA at 24 °C. The mean conductance change was 139 ± 16 pS at

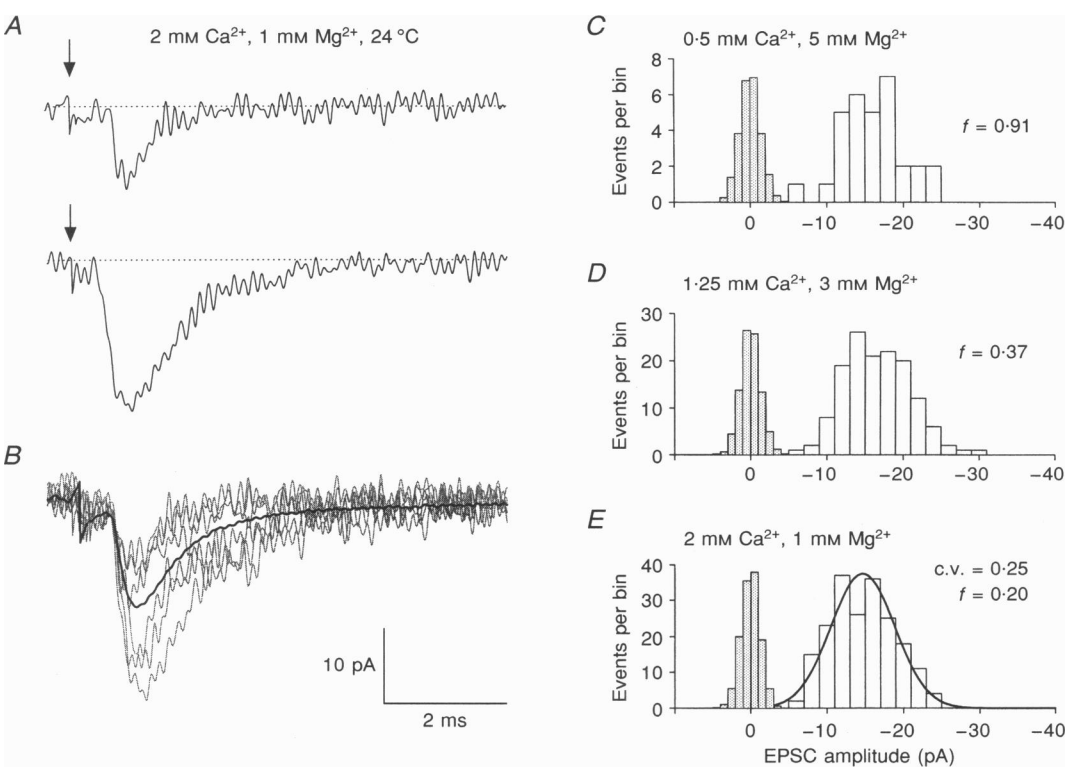

Figure 6. EPSCs from a mossy fibre–granule cell synapse with a single functional release site

A, 2 individual EPSCs from a synapse identified as having only one functional release site. The current traces were aligned on the stimulus artifact (arrow), which was reduced for clarity. *B*, 6 individual EPSCs (grey lines) aligned on their rising phase illustrate the large fluctuations about the mean (black line) of 197 EPSCs at a synapse with a single release site. *C–E*, EPSC peak amplitude distributions (open columns) and scaled background noise (shaded columns) recorded from the same synapse at −70 mV in solutions with different $[Ca^{2+}]$ and $[Mg^{2+}]$ at 24 °C. *C*, peak amplitude distribution of 31 EPSCs recorded in 0·5 mM Ca^{2+}, 5 mM Mg^{2+}; f indicates the proportion of failures. *D*, distribution of 141 EPSCs recorded in 1·25 mM Ca^{2+}, 3 mM Mg^{2+}. *E*, peak amplitude distribution of 197 EPSCs (same cell as in *A* and *B*) recorded in 2 mM Ca^{2+}, 1 mM Mg^{2+}. The distribution was well fitted by a single Gaussian function (mean = 14·7 pA, S.D. = 4·2 pA; using the maximum likelihood method).

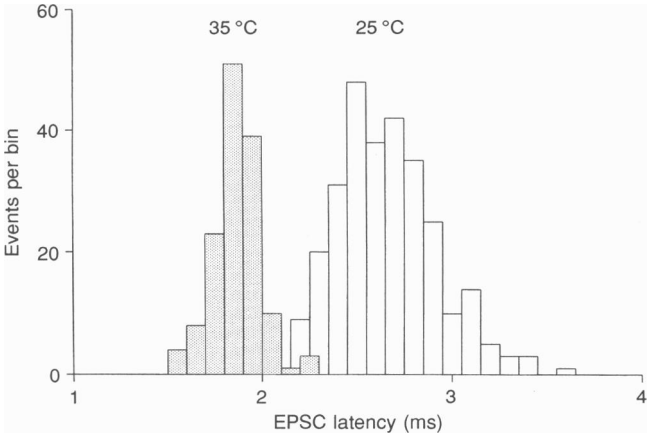

Figure 7. EPSC latency distributions for a synapse with a single functional release site

A, histograms of the EPSC latency for a single-site synapse recorded in 2 mM Ca^{2+} and 1 mM Mg^{2+} at two different temperatures. Latencies were measured between the start of the stimulus artifact and the initial rise of the EPSC. The open histogram was constructed from 284 EPSCs recorded at 25 °C and had a standard deviation of 0·27 ms. The shaded histogram was constructed from 139 EPSCs from the same synapse at 35 °C and had a standard deviation of 0·128 ms. The change in the spread of the distributions for this cell corresponded to a Q_{10} of 2·2.

24 °C ($n = 5$), increasing to 170 ± 24 pS when the temperature was raised to 35 °C ($n = 4$). Figure 6*B* illustrates the large fluctuations in the peak amplitude of single-site EPSCs. This corresponded to a mean c.v. of $0{\cdot}23 \pm 0{\cdot}02$ ($n = 5$) at 24 °C and $0{\cdot}21 \pm 0{\cdot}01$ ($n = 4$) at 35 °C (corrected for background noise). Peak amplitude distributions appeared to be independent of release probability (Fig. 6*C–D*; Kolmogorov–Smirnov test, $P > 0{\cdot}05$, $n = 5$) and were usually (4 of 5) well fitted by a single Gaussian distribution (Fig. 6*E*).

Asynchrony in the timing of transmitter release has an important influence on shaping the waveform of multi-quantal EPSCs (Isaacson & Walmsley, 1995; Diamond & Jahr, 1995). A measure of the asynchrony can be made from the single-site EPSC latency distribution. Figure 7 shows typical latency distributions for EPSCs at 25 and 35 °C from

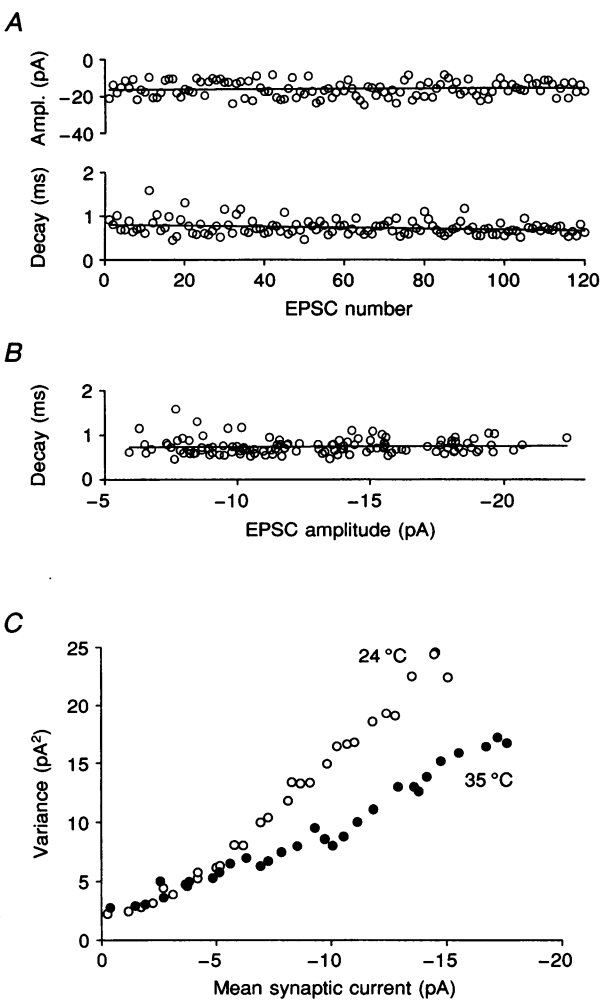

Figure 8. EPSCs from a synapse with a single release site have a non-parabolic σ^2–$\bar{I}$ relationship

A, EPSC peak amplitude and decay time course stability plots for 120 consecutive EPSCs. The decay time was the time taken to decay to 62% of peak amplitude. *B*, the relationship between decay time course and peak amplitude. The continuous lines in *A–C* are linear regression plots. None of these relationships was significantly correlated.
C, variance–mean current plot for the same synapse at 24 °C (○) and 35 °C (●). The fact that shape of the σ^2–$\bar{I}$ relationship is not a parabola suggests that the open probability of postsynaptic non-NMDA channels is not high and that the postsynaptic receptors are not saturated by transmitter. The supralinear shape of the σ^2–$\bar{I}$ plot suggests that the relationship may be distorted by variations in the amount of transmitter per packet and by a non-uniform concentration of transmitter in the synaptic cleft. The maximal variance (at the peak of the current) was consistently lower at higher temperatures as reflected in the smaller c.v.

an identified single-site synapse. Since the absolute latency (2·1 ± 0·2 ms, $n = 5$ at 24 °C; 1·1 ± 0·2 ms, $n = 4$ at 35 °C) is difficult to interpret (it will depend on the length of axon between the stimulation site and postsynaptic cell) we measured the spread of latencies. Latency distributions from single-site synapses had only one peak and had a standard deviation of 0·24 ± 0·02 ms ($n = 5$) at 24 °C. The spread of the distribution was reduced at 35 °C to 0·12 ± 0·02 ms ($n = 4$), indicating that asynchrony of transmitter release has a significant temperature dependence ($Q_{10} = 2{\cdot}4 \pm 0{\cdot}4$).

In contrast with 'saturated' multi-site synapses, stable epochs of single-site EPSCs had a linear or supralinear σ^2–$\bar{I}$ relationship (Fig. 8). The fact that the σ^2–$\bar{I}$ relationship was not parabolic suggests that the postsynaptic non-NMDA receptors were not saturated by transmitter. Quantitative information (i, N and P_o) cannot be extracted from these σ^2–$\bar{I}$ plots because they are likely to be distorted by variations in the amount of transmitter per quantum and by a non-uniform concentration of transmitter in the synaptic cleft. However, the mean conductance of channels underlying single-site EPSCs can be determined with peak-scaled non-SFA since this method is independent of variations in P_o. Figure 9*A* shows a $\sigma^2_{P\text{-}S}$–$\bar{I}$ plot for EPSCs from a single-site synapse. The conductance of channels underlying single-site EPSCs estimated with the peak-scaled non-SFA method was 11 ± 2 pS ($n = 5$) at 24 °C and 12 ± 2 pS at 35 °C ($n = 4$). This value was not different from that underlying the saturated inputs (Fig. 9*B*; 10 ± 2 pS, $n = 5$; $P > 0{\cdot}05$ also estimated with peak-scaled non-SFA) at 34 °C. It therefore seems reasonable to assume that the non-NMDA channel population is similar at single-site and saturated synapses.

At saturated synapses the parabolic shape of the $\sigma^2_{P\text{-}S}$–$\bar{I}$ relationship suggests that the channel conductance was the same thoughout the decay of the EPSC. However, when the release

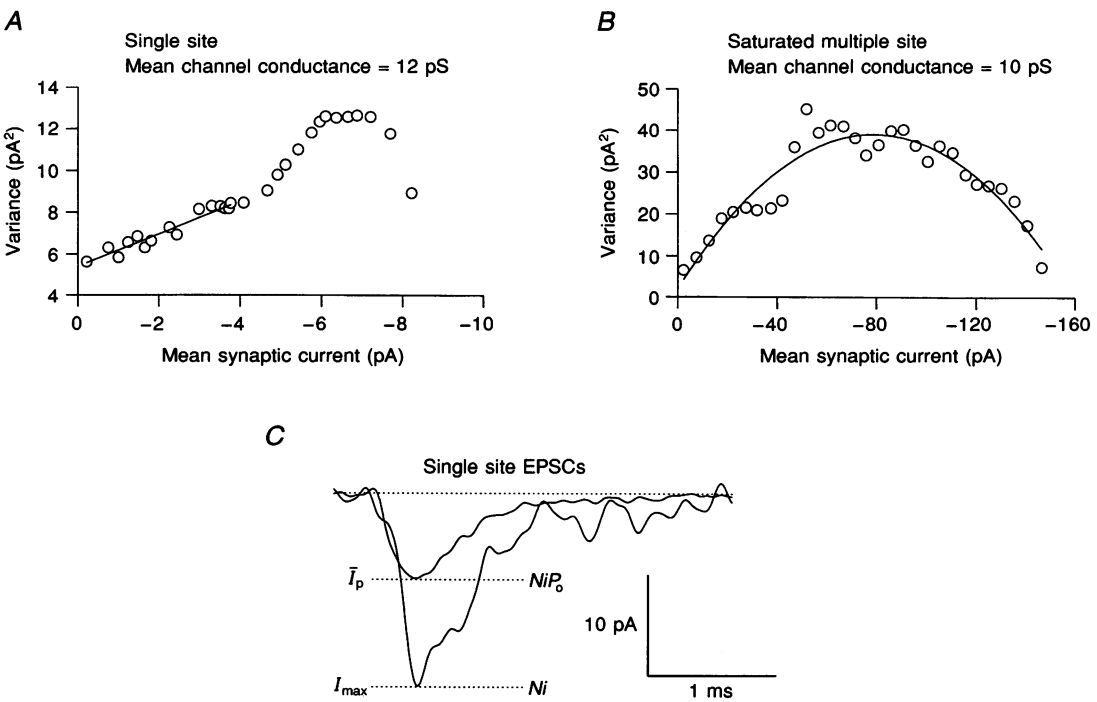

Figure 9. Estimation of channel conductance with peak-scaled non-SFA and open probability from the ratio of the mean and maximal EPSC amplitudes at 35 °C

A, peak-scaled variance–mean current ($\sigma^2_{P\text{-}S}$–$\bar{I}$) plot for 143 EPSCs from a synapse with one functional release site at 35 °C. The weighted mean single-channel current was estimated from the linear initial slope of the relationship and the conductance calculated from the mean reversal potential at this temperature. The continuous line shows a linear fit to the first 50% of the data points corresponded to a weighted mean conductance of 13 pS for this cell. *B*, peak-scaled variance–mean current plot for 41 EPSCs from a saturated multi-site synapse at 34 °C. The weighted mean single-channel current was estimated by fitting all of the data points with eqn (4) (continuous line) since the relationship was parabolic. The weighted mean channel conductance was 15 pS for this cell. *C*, method for estimating channel open probability at single-site synapses. The smaller trace shows the average of 143 evoked single-site EPSCs. The dotted line marked $\bar{I}_P$ indicates the peak of the mean current. The bigger trace shows the largest individual EPSC observed at the synapse (digitally filtered to 2·5 kHz). I_{max} is the maximum peak current observed, N is the total number of channels exposed to transmitter at the peak of the EPSC and i is the single-channel current. The ratio of $\bar{I}_P$ and I_{max} gives an upper limit for the non-NMDA channel open probability, P_o, at the peak of the EPSC.

probability was lowered the parabolic $\sigma^2_{P\text{-}S}-\bar{I}$ relationship of saturated synapses became skewed, probably as a result of channels opening after the peak of the EPSC (see Methods). Thus the skewed shape of the single-site $\sigma^2_{P\text{-}S}-\bar{I}$ relationship is likely to arise from channels opening for the first time after the peak rather than from different populations of channels with different conductances and kinetics. The mean channel conductance estimated from single-site EPSCs at 24 °C is likely to be more accurate than that from multisite synapses at 24 °C (Traynelis *et al.* 1993) because variance arising from asynchrony of transmitter release was minimal. Indeed, the non-NMDA channel conductance from single-site EPSCs is similar to that previously reported for spontaneous EPSCs (Traynelis *et al.* 1993; accounting for filter correction) where asynchrony was also minimal.

Open probability and occupancy of non-NMDA channels at single-site synapses

The number of channels exposed to transmitter (N) following the release of a quantum of transmitter can be calculated from the coefficient of variation of peak amplitude (c.v.; see Jonas *et al.* 1993; Kullmann, 1993) and the mean number of channels open at the peak of the EPSC (NP_o) since:

$$N = \frac{1}{(NP_o)^{-1} - (\text{c.v.})^2}. \quad (8)$$

NP_o (14·6 channels) was calculated from $\bar{I}_P/i$. The c.v. (0·21) was measured directly at 35 °C and gave an estimate for N of 38 channels. This calculation assumes that P_o is constant and, therefore, that the transmitter concentration is constant from one EPSC to the next. If transmitter concentration was not constant from one EPSC to the next, as seems likely, contaminating variance arising from fluctuations in the transmitter concentration will be present. The resulting increase in the c.v. will lead to a smaller denominator in eqn (8) and an overestimate of N. Because of this, estimates for P_o (0·38; from eqn (1)) and receptor occupancy ($X = 0{\cdot}45$; from eqn (2) assuming $P_{o,max} = 0{\cdot}84$) will be lower limits. Similar estimates were obtained for the data recorded at 24 °C ($N = 41$ and $P_o = 0{\cdot}31$).

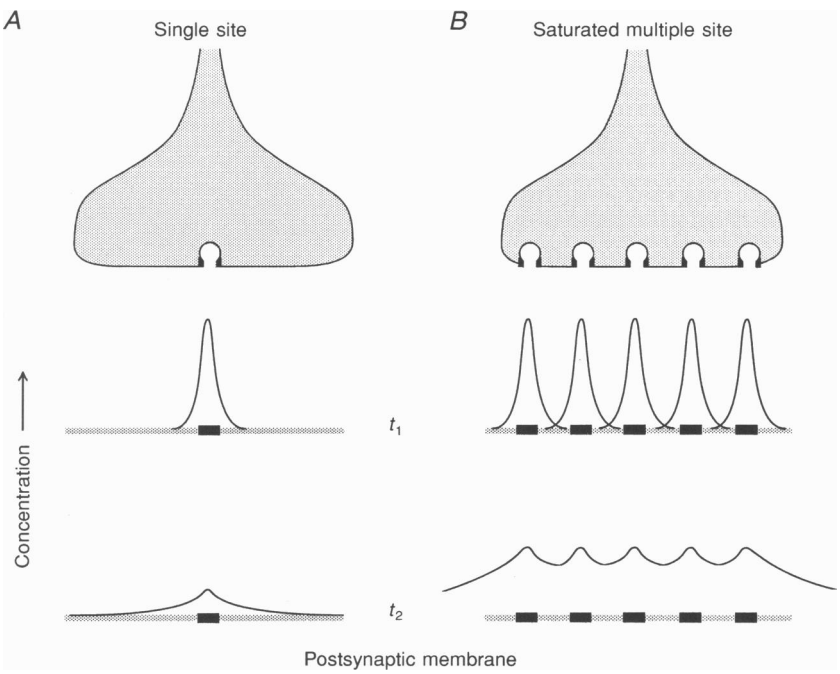

Figure 10. Schematic representation of the transmitter concentration profile at cerebellar mossy fibre–granule cell synapses at 35 °C

A, schematic diagram of a mossy fibre–granule cell synapse with one release site as a packet of transmitter is released. The black dots either side of the transmitter packet indicate the position of the release site. The middle trace represents the concentration profile of transmitter in the synaptic cleft immediately after release (t_1). The grey line indicates the postsynaptic membrane, and the black squares represent non-NMDA receptors located in the postsynaptic density (Nusser *et al.* 1994). The lower trace shows the decay and spread of concentration profile at a later time (t_2). The concentration profile of transmitter is such that only about 50% of the postsynaptic receptors become occupied by transmitter. *B*, the upper trace shows a schematic diagram of a synapse with multiple release sites as several packets of transmitter are released simultaneously. The middle trace shows the concentration profile of transmitter in the cleft immediately after release. The lower trace shows overlap of transmitter released from neighbouring sites. Changes in the transmitter concentration profile (exaggerated here for clarity) resulting from this overlap will tend to increase postsynaptic receptor occupancy. Occupancy will therefore depend on release probability at overlapping multi-site synapses.

As illustrated in Fig. 9*C*, channel open probability at a single-site synapse can also be estimated with an approach that does not assume that transmitter concentration is uniform and that does not rely on estimates of i or N. If non-NMDA receptors are close to the release site (Nusser, Mulvihill, Streit & Somogyi, 1994), so that N is constant from one EPSC to the next, P_0 can be estimated from the ratio of the mean peak EPSC amplitude ($\bar{I}_P$) and the maximal peak EPSC amplitude (I_{max}) recorded at each release site:

$$\frac{\bar{I}_P}{I_{max}} = \frac{NiP_o}{Ni} = P_o. \quad (9)$$

Because it is unlikely that all the channels were open simultaneously at the peak of the maximal EPSC, I_{max} is almost certainly a lower estimate for Ni. Thus eqns (9) and (2) will give upper limits for P_0 and occupancy. This method gave an estimate for P_0 of 0·51 ± 0·07 and an estimate of X of 0·6 ± 0·08 (range, 0·43–0·77, $n = 4$; assuming a $P_{o,max} = 0·84$) at 35 °C. Channel open probability was similar at 24 °C ($P_o = 0·48 \pm 0·04$; range, 0·34–0·58, $n = 5$). These limits for channel open probability (0·4–0·5) and receptor occupancy (0·45–0·6) indicate that release of a single packet of transmitter does not saturate the postsynaptic non-NMDA receptors at the peak of the EPSC.

A model for synaptic transmission at the mossy fibre–granule cell synapse

Comparison of our results from single-site and multiple-site synapses suggests a model for transmission at the mossy fibre–granule cell synapse at 35 °C, which is shown schematically in Fig. 10. When a single quantum of transmitter is released from a release site the concentration profile of glutamate in the cleft is such that about half of the postsynaptic non-NMDA channels become occupied by transmitter (Fig. 10*A*). When several quanta of transmitter are released simultaneously at a synapse with multiple release sites, transmitter from neighbouring sites overlaps, changing the concentration profile and presumably prolonging the presence of glutamate in the synaptic cleft (t_2, Fig. 10*B*). This results in a higher fraction of postsynaptic non-NMDA receptors being occupied by transmitter. At some synapses, overlap of transmitter produces a transmitter concentration waveform that is sufficient to saturate all of the postsynaptic non-NMDA receptors at the peak of the EPSC.

Testing the synaptic model

Our model for transmission at the mossy fibre–granule cell synapse relies on the comparison of two types of synaptic input. Implicit in this approach is the assumption that single-site and multiple-site synapses are part of the same population of synaptic inputs differing only in the number of release sites present at the synapse. Problems in our interpretation would arise if the non-NMDA receptors at single-site and saturated synapses had different apparent affinities for glutamate or different $P_{o,max}$ values as a result of developmental changes in subunit expression (Mosbacher, Schoepfer, Monyer, Burnashev, Seeburg & Ruppersberg, 1994). Two observations argue against this possibility and suggest that mossy fibre inputs are relatively homogeneous. Firstly, the weighted mean conductance of the synaptic channels underlying single-site and multi-site synapses were similar, consistent with similar synaptic non-NMDA receptor channels. Secondly, the decay time course of EPSCs from multi-site synapses recorded under low

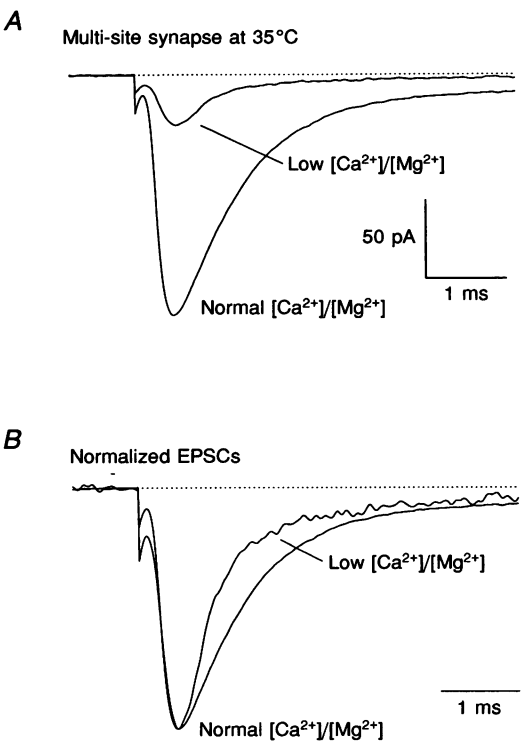

Figure 11. Lowering release probability speeds the EPSC decay at multi-site synapses

A, averaged EPSCs from a saturated multi-site synapse recorded at two different release probabilities at 35 °C (part of the stimulus artifact was omitted for clarity). The normal $[Ca^{2+}]/[Mg^{2+}]$ trace shows the average of 60 saturated EPSCs ($P_o = 0·81$) recorded in 2 mM Ca^{2+} and 1 mM Mg^{2+} which gave zero failures. The low $[Ca^{2+}]/[Mg^{2+}]$ trace shows the average of 39 EPSCs recorded from the same synapse in 0·5 mM Ca^{2+} and 5 mM Mg^{2+} which gave $f = 0·71$ and a decrease of EPSC amplitude of almost 6-fold. In both cases EPSCs were averaged by aligning on the stimulus artifact so that any asynchrony of transmitter release was included in the mean waveform. *B*, average EPSC waveforms shown in *A*, normalized to the peak. The EPSC decay became faster as the release probability was lowered at this multi-site synapse, indicating that the transmitter waveform was dependent on release probability.

probability conditions were similar to EPSCs from single-site synapses ($P > 0{\cdot}05$).

In order to test our synaptic model directly, we made specific predictions which we checked experimentally. The transmitter concentration profile in the cleft will depend on the degree of transmitter overlap between neighbouring release sites. Since the release probability (P_r) at neighbouring sites will determine the effective distance between release sites, the transmitter concentration waveform will also depend on P_r at multi-site synapses. However, this is not expected at single-site synapses as no transmitter overlap should occur. Figure 11*A* shows averaged EPSCs at 35 °C (aligned on the stimulus artifact to include asynchrony in transmitter release and excluding failures) from the same multi-site synapse under normal and low release probability conditions. The large reduction in EPSC amplitude (6-fold in this case) and increase in c.v. (~10-fold) on lowering the external $[Ca^{2+}]/[Mg^{2+}]$ ratio reflected the substantial fall in the transmitter release probability at this synapse. Figure 11*B* shows the same EPSC waveforms, normalized to peak amplitude. The decay rate of the mean EPSC became faster (35 ± 6%, $n = 7$; see Methods) as release probability was lowered. In contrast to multi-site synapses, no change occurred in the mean EPSC decay time course at single-site synapses (7 ± 8%, $n = 5$) when the $[Ca^{2+}]/[Mg^{2+}]$ ratio was reduced at 24 °C (Fig. 12*A*). It is possible that a reduction in the asynchrony of transmitter release could account for the speeding of the EPSC at multi-site synapses. We tested this by examining the latency distribution of single-site EPSCs in normal and low $[Ca^{2+}]/[Mg^{2+}]$ solutions (Fig. 12*B*). The spread of the EPSC latency distribution increased as the $[Ca^{2+}]/[Mg^{2+}]$ ratio was lowered, indicating that asynchrony of transmitter release was increased. Since this will tend to lengthen the EPSC, this change in the asynchrony of transmitter release cannot account for speeding of the EPSC decay at multi-site synapses. Changes in the asynchrony of transmitter release *between* sites will not be detected with this test but such changes are likely to be small given that the time to peak of the EPSC was independent of release probability.

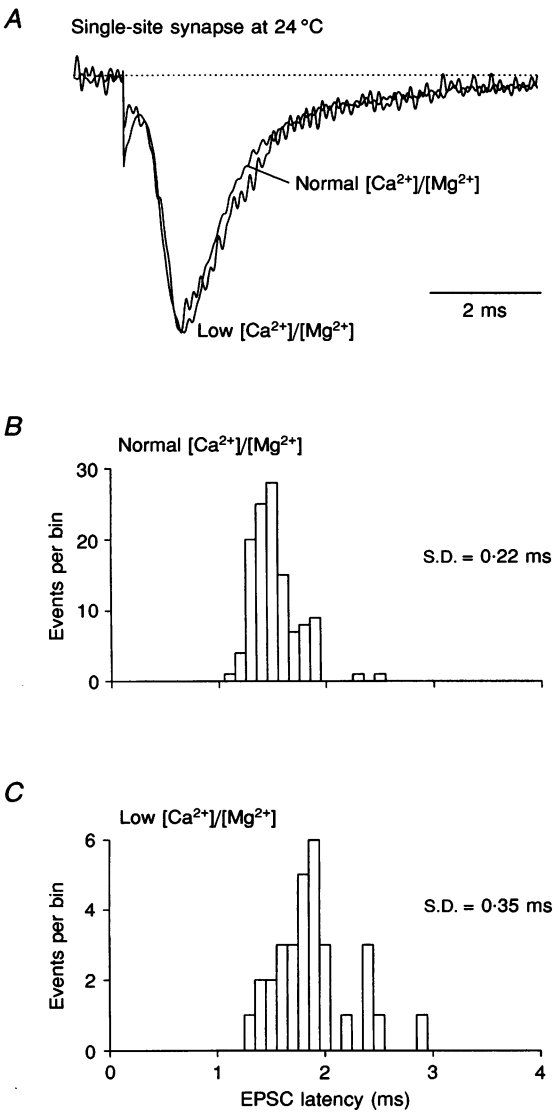

Figure 12. Lowering release probability does not change the EPSC decay at single-site synapses

A, averaged EPSCs from a single-site synapse recorded at two different release probabilities at 24 °C and normalized to the peak (part of the stimulus artifact was omitted for clarity). The normal $[Ca^{2+}]/[Mg^{2+}]$ trace shows the average of 193 EPSCs recorded in 2 mM Ca^{2+} and 1 mM Mg^{2+} which gave $f = 0{\cdot}2$. The low $[Ca^{2+}]/[Mg^{2+}]$ trace shows the average of 31 EPSCs recorded from the same synapse in 0·5 mM Ca^{2+} and 5 mM Mg^{2+} which gave $f = 0{\cdot}917$ (or $P_r = 0{\cdot}083$). Lowering the release probability did not change the shape of the EPSC. The mean EPSC amplitude did not change (+0·6%) when EPSCs were aligned on the rising phase. However a small decrease was observed when the EPSCs were aligned on the stimulus artifact. This is due to an increase in the asynchrony of transmitter release as shown in panels *B* and *C*. *B*, histogram of the EPSC latency for single-site EPSCs from the same cell recorded in 2 mM Ca^{2+} and 1 mM Mg^{2+}. *C*, histogram of the EPSC latency for single-site EPSCs from the same cell recorded in 0·5 mM Ca^{2+} and 5 mM Mg^{2+}. The standard deviation (S.D.) of the single-site EPSC latency distribution increased on average to 0·34 ± 0·02 ms ($n = 5$) as the release probability was lowered by raising Ca^{2+} and lowering Mg^{2+}. This suggests that asynchrony of transmitter release increased slightly as the release probability was lowered.

Speeding of EPSC decay at lower release probabilities suggests that the transmitter concentration profile changes with the amount of transmitter released at the multi-site synapses. This result is predicted from our model, and provides direct evidence that transmitter released from different sites can overlap in the mossy fibre–granule cell synaptic cleft.

DISCUSSION

Synapses with a single release site

Transmitter release occurs at specialized sites or active zones in the nerve terminal (Heuser, Reese & Landis, 1974). Functionally, each release site appears to behave in an all-or-none manner, releasing zero or one quantum of transmitter per presynaptic action potential (Redman, 1990; Korn & Faber, 1991). Recently, the presence of a single synaptic density has been used to identify synapses with a single release site (Gulyás *et al.* 1994). Although the morphological correlate of a release site is almost certainly a synaptic density, it is possible that a single density may have more than one functional release site. We have taken a functional approach, identifying synapses with a single release site on the basis of their release behaviour. Single-site synapses were identified as those synapses where the postsynaptic response was independent of release probability. A similar approach has been applied to hippocampal synapses (Bolshakov & Siegelbaum, 1995), although the relationship between EPSC amplitude and transmission failures was not quantified. Single-site synapses have also been identified using paired-pulse facilitation to change the release probability (Stevens & Wang, 1995; Bolshakov & Siegelbaum, 1995). However, identification of single-site synapses with this approach could be confounded if transmitter were to persist in the cleft, since postsynaptic factors, including a non-linear dose–response relationship or channel desensitization, could distort the EPSC amplitude.

Our results from identified single-site synapses indicate that non-NMDA receptors at the mossy fibre–granule cell synapse are not saturated following the release of a quantum of transmitter. The size of the postsynaptic response is therefore limited both by the amount of transmitter released in a quantum and by the number of non-NMDA channels that are exposed to the transmitter. Our estimates for channel open probability suggest that following the release of a packet of glutamate about 45–60% of the postsynaptic non-NMDA receptors become bound by transmitter and about 38–51% are open at the peak of the EPSC at 35 °C.

It should be noted that if transmitter persists in the cleft after the peak of the EPSC (Silver *et al.* 1996*a*) receptors not occupied at the peak may become bound by transmitter at later times. If the postsynaptic receptors have long-lived closed states (desensitized states) the time course of receptor occupancy and synaptic current may not be the same. Thus it is possible that the maximal occupancy does not occur at the peak of the EPSC (where our estimates were determined), but at some later time, during the decay of the synaptic current.

The range of vesicle sizes observed at the mossy fibre terminal (Palay & Chan-Palay, 1974) suggests that the number of transmitter molecules per quantum varies. Consequently, the concentration of glutamate in the synaptic cleft is also expected to vary from one quantal EPSC to the next. Estimates of P_0 and occupancy at single-site synapses are therefore likely to be mean values. The non-NMDA channel open probability at 24 °C (31–48%) was similar to that at 35 °C, but receptor occupancy is uncertain since $P_{o,max}$ is unknown for the synaptic receptor at 24 °C. Our results contrast with a recent report that non-NMDA receptors are saturated by a packet of spontaneously released glutamate at cultured synapses (Tang, Margulis, Shi & Feilding, 1994). While the high level of occupancy (~80%) reported by Tang *et al.* may have resulted from the use of cyclothiazide, as this drug increases the apparent affinity of non-NMDA receptors (Yamada & Tang, 1993) and can have presynaptic effects (Diamond & Jahr, 1995), receptor occupancy and channel open probability may not be the same at all central synapses. Indeed non-NMDA channels in different cell types have a wide range of apparent affinities for glutamate (EC_{50} values of 0·35–2 mM from rapid perfusion of membrane patches; Jonas & Sakmann, 1992; Raman & Trussell, 1992). Heterogeneity in the subunit composition of non-NMDA receptors could underlie these different EC_{50} values for glutamate and result in different levels of receptor occupancy both during development and at different central synapses.

Our analysis at single-site mossy fibre–granule cell synapses suggests that an average of thirty to forty channels are exposed to transmitter at the peak of the EPSC. If non-NMDA channels were distributed over a relatively wide postsynaptic area, estimates of N for the single-site synapse would be underestimated (and P_0 overestimated) since the diffusion time from the release site to the receptors may be longer than the time to peak of the EPSC. Although the precise subsynaptic distribution of the postsynaptic receptors cannot be deduced from our approach, a recent immunohistochemical study indicates that the postsynaptic non-NMDA receptors are located within postsynaptic densities at the mossy fibre–granule cell synapse (Nusser *et al.* 1994). It is also of note that non-NMDA channels are not present on the soma of granule cells in thin slices (Silver *et al.* 1996*a*). It therefore seems likely that non-NMDA channels are restricted to the postsynaptic density apposing each release site (see Fig. 10). If all of the thirty to forty non-NMDA channels are present within the 0·1 μm radius of the synaptic density (Nusser *et al.* 1994) their packing density will be about 1000 μm^{-2}. This value is of the same order as that for particles within synaptic densities in other cell types (2000–4000 μm^{-2}; Harris & Landis, 1986).

The EPSC amplitude distributions from single-site synapses were usually well fitted by a single Gaussian function (Fig. 6*E*) as has been observed for morphologically identified single-site synapses in the hippocampus (Gulyás *et al.* 1994), and for minimal inhibitory synaptic currents evoked under low release probability conditions (Takahashi, 1992). However, as at many other synapses (Takahashi, 1992; Raastad *et al.* 1992; Hestrin, 1992; Jonas *et al.* 1993; Paulsen & Heggelund, 1994; Tang *et al.* 1994) granule cell miniature EPSC distributions recorded in tetrodotoxin have a distinct skew toward larger events (Silver *et al.* 1992). The mean conductance change and mean c.v. of single-site EPSCs were not different from the corresponding values from the main component of the miniature EPSC amplitude distributions in granule cells ($P > 0{\cdot}05$ for both cases; 120 ± 30 pS and $0{\cdot}23 \pm 0{\cdot}01$, $n = 4$, from multiple Gaussian fits; R. A. Silver, S. F. Traynelis & S. G. Cull-Candy, unpublished observations). The spontaneous release of a quantum of glutamate from individual release sites could therefore account for the smallest amplitude component of the miniature EPSC distributions, although the origin of the larger events remains unclear.

Saturation at multi-site synapses

Our results indicate that at some mossy fibre–granule cell synapses with multiple release sites, the postsynaptic non-NMDA receptors are saturated by transmitter. The size of the synaptic current at these inputs appears to be limited by the number of postsynaptic channels rather than by the amount of transmitter released. Application of non-stationary fluctuation analysis to 'saturated' synaptic inputs has allowed us to estimate directly the total number of postsynaptic channels exposed to transmitter (at the peak of the EPSC) at these multi-site synapses. Non-SFA indicates that an average of 170 non-NMDA channels are located in the postsynaptic membrane of these inputs. This would correspond to an average of about five synaptic densities if single-site and saturated inputs have a similar mean number of channels per postsynaptic density. However, the wide variation in N (60–310) that we observed at saturated multi-site synapses may reflect differences both in the number and size of the synaptic densities present.

Non-SFA of saturated synaptic inputs also provides the first direct estimate of $P_{o,max}$ for the synaptic non-NMDA channel. Previous estimates for the $P_{o,max}$ of extrasynaptic non-NMDA channels in outside-out membrane patches gave values of 0·5–0·7 at room temperature (Jonas *et al.* 1993; Hestrin, 1992; Spruston *et al.* 1995). Although our estimate for the postsynaptic channels at 34 °C is higher (0·84) it may in fact be a lower limit because any deviation from full transmitter saturation will give an underestimate with our method of analysis. The smaller estimates for $P_{o,max}$ obtained from patches could be due to receptor heterogeneity, but may simply reflect differences in temperature or limitations in the speed of glutamate application.

Transmitter overlap raises receptor occupancy at multi-site synapses

Our experiments suggest that transmitter released from neighbouring sites overlaps within the synaptic cleft (Fig. 10*B*) and that the fraction of the postsynaptic channels occupied by transmitter depends on the amount of transmitter released at multi-site synapses. It is likely that a change in release probability at multi-site synapses alters the level of receptor occupancy by changing both the concentration of transmitter and the length of time transmitter remains in the cleft. Overlap of transmitter in the synaptic cleft has been proposed at the NMJ when cholinesterase activity is inhibited (Hartzell *et al.* 1975) and at avian auditory synapses (Trussell *et al.* 1993), but its effect on postsynaptic receptor occupancy has not previously been determined. Transmitter overlap is also thought to occur between neighbouring synapses (Faber & Korn, 1988; Tong & Jahr, 1994; Barbour *et al.* 1994; Mennerick & Zorumski, 1995) but this may occur only when a large number of synaptic inputs are synchronously activated. The degree of transmitter overlap will depend both on P_r and the diffusion distance between neighbouring release sites. If each synaptic density at the mossy fibre–granule cell synapse corresponds to a release site (average separation, 0·6–0·7 μm; estimated from Hámori & Somogyi, 1983), glutamate concentration would be expected to peak at neighbouring sites in about 120 μs at 35 °C (see Methods), which is well within the time to peak of the saturating EPSCs (460 ± 40 μs, $n = 5$). At this distance from the release site the dilution of transmitter concentration will be relatively large, so the summation in transmitter concentration observed at saturating inputs would suggest that sites are closer than this mean value. The behaviour of synaptic connections where overlap of transmitter occurs is expected to differ from the all-or-none behaviour of synapses where synaptic densities are independent (Perkel & Nicoll, 1993). If the density of release sites at a multi-site synapse is high, overlap of transmitter could result in a super-saturating concentration of glutamate in the synaptic cleft. Overlap of transmitter may therefore permit full receptor occupancy at a multi-site synapses when the probability of release at each site is less than 1.

It is likely that the signal processing characteristics of mossy fibre inputs with a single release site will be very different from those which are saturated by transmitter. If only one 'saturating' mossy fibre is necessary to fire a granule cell then the synapse will act as a one-to-one relay, but if multiple- inputs are necessary, saturation of the postsynaptic receptors may allow reproducible synaptic integration at a small number of synaptic inputs. It remains to be seen whether the different number of release sites observed at mossy fibre inputs (and therefore the synaptic efficacy) arises either from plasticity in the synaptic connections, or represents a genetically pre-set weighting of

different synapse, or whether they reflect different stages of synaptic development in the immature animal. Resolution of these points will provide a more thorough understanding of signal processing at the mossy fibre–granule cell synapse and cerebellar function as a whole.

Barbour, B., Keller, B. U., Llano, I. & Marty, A. (1994). Prolonged presence of glutamate during excitatory synaptic transmission to cerebellar Purkinje cells. *Neuron* **12**, 1331–1343.

Bekkers, J. M., Richerson, G. B. & Stevens, C. F. (1990). Origin of variability in quantal size in cultured hippocampal neurons and hippocampal slices. *Proceedings of the National Academy of Sciences of the USA* **87**, 5359–5362.

Bolshakov, V. Y. & Siegelbaum, S. A. (1995). Regulation of hippocampal transmitter release during development and long-term potentiation. *Science* **269**, 1730–1734.

Brickley, S. G., Farrant, M. & Cull-Candy, S. G. (1995). Single-channel conductance of synaptically activated $GABA_A$ receptors in rat cerebellar granule cells in slices. *Journal of Physiology* **483.P**, 60–61*P*.

Colquhoun, D. & Sigworth, F. J. (1995). In *Single-Channel Recording*, 2nd edn, ed. Sakmann, B. & Neher, E., pp. 483–587. Plenum Press, London.

Crank, J. (1975). In *The Mathematics of Diffusion*, pp. 28–29. Oxford University Press, UK.

Del Castillo, J. & Katz, B. (1957). Interaction at end-plate receptors between different choline derivatives. *Proceedings of the Royal Society* B **146**, 369–381.

Diamond, J. S. & Jahr, C. E. (1995). Asynchronous release of synaptic vesicles determines the time course of the AMPA receptor-mediated EPSC. *Neuron* **15**, 1097–1107.

Eccles, J. C., Ito, M. & Szentagothai, J. (1967). In *The Cerebellum as a Neuronal Machine*, pp. 116–130. Springer-Verlag, Germany.

Edwards, F. A., Konnerth, A., Sakmann, B. & Takahashi, T. (1989). A thin slice preparation for patch-clamp recordings from neurones of the mammalian central nervous system. *Pflügers Archiv* **414**, 600–612.

Faber, D. S. & Korn, H. (1988). Synergism at central synapses due to lateral diffusion of transmitter. *Proceedings of the National Academy of Sciences of the USA* **85**, 8708–8712.

Frankenhaeuser, B. & Hodgkin, A. L. (1957). The actions of calcium on the electrical properties of squid axons. *Journal of Physiology* **137**, 218–244.

Gulyás, A. I., Miles, R., Sík, A., Tóth, K., Tamamakl, N. & Freund, T. F. (1994). Hippocampal pyramidal cells excite inhibitory neurons through a single release site. *Nature* **366**, 683–687.

Hámori, J. & Somogyi, J. (1983). Differentiation of cerebellar mossy fiber synapses in the rat: a quantitative electron microscope study. *Journal of Comparative Neurology* **220**, 365–377.

Harris, K. M. & Landis, D. M. D. (1986). Membrane structure at synaptic junctions in area CA1 of the rat hippocampus. *Neuroscience* **19**, 857–872.

Hartzell, H. C., Kuffler, S. W. & Yoshikarmi, D. (1975). Post-synaptic potentiation: interaction between quanta of acetylcholine at the skeletal neuromuscular synapse. *Journal of Physiology* **251**, 427–463.

Hestrin, S. (1992). Activation and desensitization of glutamate-activated channels mediating fast excitatory synaptic currents in the visual cortex. *Neuron* **9**, 991–999.

Heuser, J. E., Reese, T. S. & Landis, D. M. D. (1974). Functional changes in frog neuromuscular junctions studied with freeze-fracture. *Journal of Neurocytology* **3**, 109–131.

Hollmann, M. & Heinemann, S. (1994). Cloned glutamate receptors. *Annual Review of Neuroscience* **17**, 31–108.

Isaacson, J. S. & Walmsley, B. (1995). Counting quanta: Direct measurements of transmitter release at a central synapse. *Neuron* **15**, 875–884.

Jack, J. J. B., Redman, S. J. & Wong, K. (1981). The components of synaptic potentials evoked in cat spinal motoneurones by impulses in single group I a afferents. *Journal of Physiology* **321**, 65–96.

Jakab, R. L. & Hámori, J. (1988). Quantitative morphology and synaptology of cerebellar glomeruli in the rat. *Anatomy and Embryology* **179**, 81–88.

Jonas, P., Major, G. & Sakmann, B. (1993). Quantal components of unitary EPSCs at the mossy fibre synapse on CA3 pyramidal cells of rat hippocampus. *Journal of Physiology* **472**, 615–663.

Jonas, P. & Sakmann, B. (1992). Glutamate receptor channels in isolated patches from CA1 and CA3 pyramidal cells of rat hippocampal slices. *Journal of Physiology* **455**, 143–171.

Jonas, P. & Spruston, N. (1994). Mechanisms shaping glutamate-mediated excitatory postsynaptic currents in the CNS. *Current Opinion in Neurobiology* **4**, 366–372.

Kamboj, S. K., Swanson, G. T. & Cull-Candy, S. G. (1995). Intracellular spermine confers rectification on rat calcium-permeable AMPA and kainate receptors. *Journal of Physiology* **486**, 297–303.

Katz, B. (1969). *The Release of Neural Transmitter Substances.* Liverpool University Press, UK.

Koh, D.-S., Burnashev, N. & Jonas, P. (1995). Block of native Ca^{2+}-permeable AMPA receptors in rat brain by intracellular polyamines generates double rectification. *Journal of Physiology* **486**, 305–312.

Korn, H. & Faber, D. S. (1991). Quantal analysis and synaptic efficacy in the CNS. *Trends in Neurosciences* **14**, 439–445.

Kullmann, D. M. (1993). Quantal variability of excitatory transmission in the hippocampus: implications for the opening probability of fast glutamate-gated channels. *Proceedings of the Royal Society* B **253**, 107–116.

Kullmann, D. M. & Nicoll, R. A. (1992). Long-term potentiation is associated with increases in quantal content and quantal amplitude. *Nature* **357**, 240–244.

Kuno, M. & Takahashi, T. (1986). Effects of calcium and magnesium on transmitter release at I a synapses of rat spinal motoneurones *in vitro*. *Journal of Physiology* **376**, 543–553.

Larkman, A., Stratford, K. & Jack, J. (1991). Quantal analysis of excitatory synaptic action and depression in hippocampal slices *Nature* **350**, 344–347.

Mennerick, S. & Zorumski, C. F. (1995). Presynaptic influence on the time course of fast excitatory synaptic currents in cultured hippocampal cells. *Journal of Neuroscience* **15**, 3178–3192.

Mosbacher, J., Schoepfer, R., Monyer, H., Burnashev, N., Seeburg, P. H. & Ruppersberg, J. P. (1994). A molecular determinant for submillisecond desensitization in glutamate receptors. *Science* **266**, 1059–1062.

Nusser, Z., Mulvihill, E., Streit, P. & Somogyi, P. (1994). Subsynaptic segregation of metabotropic and ionotropic glutamate receptors as revealed by immunogold localization. *Neuroscience* **61**, 421–427.

Palay, S. L. & Chan-Palay, V. (1974). In *Cerebellar Cortex: Cortex and Organization*. Springer-Verlag, Germany.

Paulsen, O. & Heggelund, P. (1994). The quantal size at retinogeniculate synapses determined from spontaneous and evoked EPSCs in guinea-pig thalamic slices. *Journal of Physiology* **480**, 505–511.

Perkel, D. J. & Nicoll, R. A. (1993). Evidence for all-or-none regulation of neurotransmitter release: implications for long-term potentiation. *Journal of Physiology* **471**, 481–500.

Press, W. H., Teukolsky, S. A. Vetterling, W. T. & Flannery, B. P. (1994). In *Numerical Recipes in C*, pp. 623–626. Cambridge University Press, UK.

Raastad, M., Storm, J. F. & Andersen, P. (1992). Putative single quantum and single fibre excitatory postsynaptic currents show similar amplitude range and variability in rat hippocampal slices. *European Journal of Neuroscience* **4**, 113–117.

Raman, I. M. & Trussell, L. O. (1992). The kinetics of the response to glutamate and kainate in neurons of the avian cochlear nucleus. *Neuron* **9**, 173–186.

Redman, S. (1990). Quantal analysis of synaptic potentials in neurons of the central nervous system. *Physiological Reviews* **70**, 165–198.

Seeburg, P. H. (1993). The molecular biology of mammalian glutamate receptor channels. *Trends in Neurosciences* **16**, 359–364.

Sigworth, F. J. (1980). The variance of sodium current fluctuations at the node of Ranvier. *Journal of Physiology* **307**, 97–129.

Silver, R. A., Colquhoun, D., Cull-Candy, S. G. & Edmonds, B. (1996*a*). Deactivation and desensitization of non-NMDA receptors in patches and the time course of EPSCs in rat cerebellar granule cells. *Journal of Physiology* **493**, 167–173.

Silver, R. A., Cull-Candy, S. G. & Takahashi, T. (1994). A model for synaptic transmission at the rat cerebellar mossy fibre–granule cell synapse deduced from non-stationary fluctuation analysis. *Journal of Physiology* **477.P**, 93*P*.

Silver, R. A., Cull-Candy, S. G. & Takahashi, T. (1995). Non-NMDA receptor occupancy during transmission at rat cerebellar mossy fibre–granule cell synapses with only one functional release site. *Journal of Physiology* **489.P**, 16*P*.

Silver, R. A., Farrant, M. & Cull-Candy, S. G. (1996*b*). Filtering of synaptic currents estimated from the time course of NMDA channel opening at the rat cerebellar mossy fibre–granule cell synapse. *Journal of Physiology* (in the Press).

Silver, R. A., Traynelis, S. F. & Cull-Candy, S. G. (1992). Rapid-time-course miniature and evoked excitatory currents at cerebellar synapses *in situ*. *Nature* **355**, 163–166.

Spruston, N., Jonas, P. & Sakmann, B. (1995). Dendritic glutamate receptor channels in rat hippocampal CA3 and CA1 pyramidal neurons. *Journal of Physiology* **482**, 325–352.

Stevens, C. F. & Wang, Y. (1995). Facilitation and depression at single central synapses. *Neuron* **14**, 795–802.

Takahashi, T. (1992). The minimal inhibitory synaptic currents evoked in neonatal rat motoneurones. *Journal of Physiology* **450**, 593–611.

Tang, C.-M., Margulis, M., Shi, Q.-Y. & Feilding, A. (1994). Saturation of postsynaptic glutamate receptors after quantal release of transmitter. *Neuron* **13**, 1385–1393.

Tong, G. & Jahr, C. E. (1994). Multivesicular release from excitatory synapses of cultured hippocampal neurons. *Neuron* **12**, 51–59.

Traynelis, S. F., Silver, R. A. & Cull-Candy, S. G. (1993). Estimated conductance of glutamate receptor channels activated during EPSCs at the cerebellar mossy fibre-granule cell synapse *Neuron* **11**, 279–289.

Trussell, L. O., Zhang, S. & Raman, I. M. (1993). Desensitization of AMPA receptors upon multiquantal neurotransmitter release. *Neuron* **10**, 1185–1196.

Wyllie, D. J. A., Traynelis, S. F. & Cull-Candy, S. G. (1993). Evidence for more than one type of non-NMDA receptor in outside-out patches from cerebellar granule cells of the rat. *Journal of Physiology* **463**, 193–226.

Yamada, K. A. & Tang, C.-M. (1993). Benzothiadiazides inhibit rapid glutamate receptor desensitization and enhance glutamatergic synaptic currents. *Journal of Neuroscience* **13**, 3904–3915.

Acknowledgements

This work was supported by The Wellcome Trust and the Monbusho International Scientific Research Program of Japan. S.G.C.-C.'s research programme is supported in part by an International Research Scholars Award from the Howard Hughes Medical Institute. T.T.'s research programme is supported in part by a Grant-in-Aid for Scientific Research from the Ministry of Education, Science and Culture of Japan. We thank David Attwell, Brian Edmonds, Mark Farrant, Bernard Katz, Motoy Kuno and David Rossi for helpful discussion and comments on the manuscript and David Colquhoun, Stephen Traynelis and Iuona Vais for generously providing software.

Authors' email addresses

R. A. Silver: a.silver@ucl.ac.uk

S. G. Cull-Candy: s.cull-candy@ucl.ac.uk

T. Takahashi: ttakahas-tky@umin.u-tokyo.ac.jp

Received 6 November 1995; accepted 27 February 1996.